Physics of Fluids

Nonlinear evolution of interacting sinuous and varicose modes in plane wakes and jets: Quasi-periodic structures

Cite as: Phys. Fluids **32**, 064104 (2020); https://doi.org/10.1063/5.0007019
Submitted: 08 March 2020 . Accepted: 04 May 2020 . Published Online: 18 June 2020

Kirill Mikhaylov, and Xuesong Wu

View Online Export Citation CrossMark

ARTICLES YOU MAY BE INTERESTED IN

Acoustic-wave-induced cooling in onset of hypersonic turbulence
Physics of Fluids **32**, 061702 (2020); https://doi.org/10.1063/5.0011871

Effect of surfactant and evaporation on the thin liquid film spreading in the presence of surface acoustic waves
Physics of Fluids **32**, 062106 (2020); https://doi.org/10.1063/5.0007902

Resistance of velocity slip flow in pipe/channel with a sudden contraction
Physics of Fluids **32**, 063602 (2020); https://doi.org/10.1063/5.0009415

AIP Publishing
NEW: TOPIC ALERTS
Explore the latest discoveries in your field of research
SIGN UP TODAY!

AIP Publishing

© 2020 Author(s).

Physics of Fluids ARTICLE scitation.org/journal/phf

Nonlinear evolution of interacting sinuous and varicose modes in plane wakes and jets: Quasi-periodic structures

Cite as: Phys. Fluids 32, 064104 (2020); doi: 10.1063/5.0007019
Submitted: 8 March 2020 • Accepted: 4 May 2020 •
Published Online: 18 June 2020

View Online Export Citation CrossMark

Kirill Mikhaylov[1] and Xuesong Wu[2,a),b)]

AFFILIATIONS

[1] Department of Aeronautics, Imperial College London, London SW7 2AZ, United Kingdom
[2] School of Mechanical Engineering, Nantong University, Nantong 226019, China

[a)] **Author to whom correspondence should be addressed:** x.wu@ic.ac.uk
[b)] On leave from Department of Mathematics, Imperial College London, London SW7 2AZ, United Kingdom.

ABSTRACT

A plane wake or jet supports sinuous and varicose instability modes. The nonlinear interaction between them following their linear development was described previously by Leib and Goldstein ["Nonlinear interaction between the sinuous and varicose instability modes in a plane wake," Phys. Fluids A **1**, 513–521 (1989)] using the strongly nonlinear non-equilibrium critical-layer approach in the case of the Bickley jet for which the frequencies of the sinuous and varicose modes have an integer ratio of 2. This paper develops the theory for general profiles where the frequencies of the sinuous and varicose modes are non-commensurable. The disturbance is quasi-periodic in time and space and must be expressed as a function of two phase variables. Using matched asymptotic expansions simultaneously with the multi-scale method, we derived a set of coupled evolution equations governing the development of the amplitudes and critical-layer vorticities of these modes. The evolution system is solved for the base-flow profiles mimicking those in experiments. The sinuous mode suppresses the varicose mode but also causes the latter to saturate in a highly oscillatory manner. The varicose mode inhibits the sinuous mode initially. However, in the later stage, it lends the sinuous mode a significantly higher saturating amplitude. For a wide range of initial modal compositions and Reynolds numbers, the ratio of the varicose mode amplitude to that of the sinuous mode eventually tends to an almost constant value in the range of 0.4–0.6, in line with the experimental measurement. Due to the self and mutual interactions, the vorticities roll up to form vortices, which are non-symmetric in the transverse direction and quasi-periodic in the streamwise direction as well as in time. With such an increased complexity, the vortices resemble those observed in experiments. The nonlinear interactions of the sinuous and varicose modes in the critical layer generate all harmonics in the main layer, as a result of which the perturbation is non-periodic and may even appear "random-like."

Published under license by AIP Publishing. https://doi.org/10.1063/5.0007019

I. INTRODUCTION

Understanding the nonlinear behavior of a plane wake or jet that undergoes transition to turbulence is important for many scientific and technological applications. Examples include atmospheric and oceanographic wakes and jets, where nonlinear effects control the momentum transport, and chemical engineering applications, where they have a significant impact on the entrainment and mixing of chemical species.[1,2] In jets, nonlinear wavepackets of instability modes are known to be the important sources of noise.[3]

Plane wakes and jets are both boundary-layer types of flows. They evolve slowly in the streamwise direction with the streamwise velocity being much greater than the transverse component. As the streamwise velocity profiles of these flows are inflectional, they support essentially inviscid Rayleigh instability waves that evolve downstream. The characteristic wavelength and amplification rate of the instability waves can initially be well described by linear stability theory, i.e., by solving the Rayleigh or Orr–Sommerfeld equation, which can be derived based on the assumption of a locally parallel flow.[4–6] Due to the symmetry of the profile, sinuous and varicose

Published under license by AIP Publishing

modes are identified, whose transverse velocity eigenfunctions are symmetric and antisymmetric, respectively. The sinuous mode has a larger amplification rate and amplifies in a broader frequency range.[7] Calculations were performed for the base-flow profiles that closely resemble the measured ones, and the predictions were found to be in reasonable agreement with experiments.[4,5,7] Despite its smaller growth rate, the varicose mode is also present and co-exists with the sinuous mode. As the perturbations grow, nonlinear effects become significant. The self-interaction of each mode generates the mean-flow distortion and harmonics.[4,8,9] Furthermore, mutual interactions of modes with different frequencies, ω_1 and ω_2 say, excite components with combination frequencies $m\omega_1 + n\omega_2$, where m and n are integers, the development of which gradually fills up the spectrum of the disturbance, causing flow randomization.[8,10,11] In particular, when $(\omega_1 - \omega_2)$ is small, the difference-frequency component acquires an exceptionally large amplitude, and the phase and amplitude of the disturbance appear to be modulated on the long time scale inversely proportional to $O(\omega_1 - \omega_2)$.[8,9] As a result of these nonlinear interactions, the amplitudes deviate from the quasi-exponential growth and saturate in a rather complex (oscillatory) manner, and the initially sinusoidal perturbation rolls up to form concentrated vortices.[2,12,13]

Large-scale disturbances, akin to instability waves or vortices, have been observed experimentally in fully turbulent wakes[14,15] and jets[16,17] as well as in mixing layers,[18] when these flows are subject to external time-periodic excitations. Such orderly disturbances are referred to as coherent structures. They undergo amplification, saturation, and eventual attenuation. It has also been demonstrated that the earlier evolution of these coherent structures can be modeled as instability modes of the time-averaged mean-flow profiles,[14,15,17] as was demonstrated earlier for the circular jet.[19] However, approaching the neutral position, the structures cannot be predicted by a linear instability analysis as nonlinear effects come into play. In the unexcited case, the frequency of the locally predominant (i.e., the most energetic) components in the fluctuation spectrum corresponds to the frequency of the instability mode that is locally neutral.[15,20]

The continued development following the linear stage was first studied by Liu[21] and Maslowe[22] in the framework of the classical weakly nonlinear theory of Stuart–Watson–Landau.[23,24] The nonlinear evolution is deemed to take place on the length scale of $O(\varepsilon^{-2})$, where ε is a measure of the amplitude of the mode. For non-parallelism to be negligible, it is required that $\varepsilon^{-2} \ll R^{1/2}$, while $\varepsilon^{1/2} \ll R^{-1/3}$ must be assumed in order to avoid the strongly nonlinear critical-layer dynamics, where R denotes the Reynolds number based on the shear-layer thickness. These two requirements are unfortunately contradictory.

An alternative heuristic approach was developed in Refs. 25 and 26 where the integral forms of both the perturbation kinetic energy and momentum equations in conjunction with the prescribed self-similar mean-flow profile and the assumption that the mode retains its transverse shape given by the eigenfunction were employed to derive the coupled equations governing the modal amplitude, the shear-layer thickness, and the velocity deficit of the wake. This theory captures the evolution of these quantities.[26,27] However, it cannot describe the generation of harmonics or vortex roll-up. The nonlinear spatial–temporal development of a sinuous mode in the long-wavelength limit, which pertains to the vicinity of the trailing edge, was investigated using the high-Reynolds-number asymptotic approach.[28]

In a spatially developing flow such as a wake or jet, a small-amplitude mode with a given frequency would become neutral at a streamwise position. Since the mode has acquired its maximum amplitude through the accumulated exponential amplification, nonlinear effects are likely to become important. Churilov and Shukhman[29] and Huerre[30] considered the nonlinear evolution of a nearly neutral mode with amplitude $\varepsilon = O(R^{-1})$. They pointed out that in the large-Reynolds-number limit, the dominant nonlinear effect came from the critical layer, a thin region surrounding the transverse level, at which the base-flow velocity is equal to the phase speed of the mode. Within the critical layer, the dynamics of the disturbance is viscous and weakly nonlinear in that the mode interacts with itself to generate a mean-flow distortion, which contributes a stabilizing nonlinear effect. With a small $O(R^{-1})$ amplitude, the nonlinear evolution length scale was of $O(\varepsilon^{-5/3})$, which is much shorter than $O(\varepsilon^{-2})$ in Refs. 21 and 22 but is still far too long for non-parallelism to be neglected. The evolution of a nearly neutral mode in the strongly nonlinear viscous critical-layer regime was first considered by Huerre,[31] and the threshold amplitude of the mode is $O(R^{-2/3})$. However, the evolution was taken to be over an $O(R)$ length, apparently for the sake of accounting for a weak viscosity related (nonlinear) effect. In both of the analyses,[30,31] a body force had to be introduced to suppress the non-parallelism. This practice, which renders the problem artificial, can be avoided because nonlinearity and non-parallelism can be treated consistently by considering evolution that may naturally take place on a shorter length scale. Two distinguished regimes are of interest. The first pertains to a mode having an $\varepsilon = O(R^{-2/3})$ amplitude and evolving an $O(R^{1/2})$ length scale through the neutral position. This regime has not received much attention but is distinguished in that non-parallelism plays a leading-order role while the critical-layer dynamics is viscous and strongly nonlinear but in equilibrium (which refers to fact that the slow variation of the modal amplitude does not appear at leading order in the critical-layer equations).

The second and more interesting is the non-equilibrium strongly nonlinear critical-layer regime, which commences in the region at $O(\varepsilon^{1/2}R)$ distances upstream of the neutral position. In that region, the deviation of the normalized frequency from the local neutral value is $O(\varepsilon^{1/2})$,[32,33] and the mode evolves nonlinearly on the rather short length scale of $O(\varepsilon^{-1/2})$, which is of $O(R^{-1/3})$ or shorter. It follows that the non-parallelism is now, indeed, negligible, but importantly the non-equilibrium effect, associated with the slow variation of the modal amplitude, appears at leading order in the critical layer. The nonlinear theory in this regime, first formulated by Goldstein and Leib[32] and Goldstein and Hultgren,[33] captures very well the nonlinear saturation and vortex roll-up.

In nonlinear, non-equilibrium critical-layer theory, the disturbance in the main part of the shear layer is linear and inviscid, and an outer solution that is valid outside of the critical layer is obtained. Nonlinear interactions take place within the critical layer, and an inner solution is constructed, which is valid there. By matching the outer and inner solutions, the evolution equations governing the amplitude and critical-layer vorticity of the disturbance were derived; a recent review of the topic was given by Wu.[34]

In the case of a wake or jet, the sinuous mode has a greater amplification rate than the varicose mode because of which the

Published under license by AIP Publishing

latter was often neglected. In reality, they co-exist. This is supported by both direct numerical simulation (DNS) data[13] and flow visualization,[2,14] which indicate that the disturbances do not exhibit the otherwise expected symmetry. Moreover, it has been observed that the varicose mode can dominate the shape of the large structures[35] and alter the gross behavior of the streakline patterns even if the sinuous mode is dominant.[14] Mutual interactions are expected to take place when one or two modes acquire a significant amplitude. Marasli *et al.*[15] decomposed the disturbance into varicose and sinuous modes and found that the former has an amplitude twice that of the latter in the upstream region, and the ratio tended to 0.5 sufficiently downstream. These authors also attributed the lack of universality of the self-preserving wake to the interaction of the varicose and sinuous modes. The amplitudes of these modes are dependent, in practice, on the receptivity and may also be selected by controlled excitations.[14,15,36]

The theory developed for a single mode in a free shear layer[32,33] was extended by Leib and Goldstein[37] to nonlinearly interacting sinuous and varicose modes in a plane wake. The velocity profile was chosen to be the so-called "Bickley jet," which is somewhat special in that the varicose mode has the neutral frequency exactly double that of the sinuous mode. This leads to a significant simplification of the formulation. With the varicose mode being the exact subharmonic of the sinuous mode, the disturbance is periodic in time and in the streamwise coordinate moving with the phase speed of the modes. The formulation in Refs. 32 and 33 was also extended to a more general form of disturbance, namely, a modulated wavetrain,[38] which consists of a discrete number, or a continuum, of modes with frequencies that are close to each other. Further downstream, three-dimensional disturbances develop rapidly. Nonlinear, non-equilibrium critical layer theory has also been used to describe the resonant triad interactions among a planar sinuous-mode, an oblique sinuous-mode, and an oblique varicose-mode.[39] The predicted that nonlinear dynamics was consistent with the experimental observations further downstream.

In this study, we investigate the nonlinear interactions of two-dimensional (2D) sinuous and varicose modes in more realistic base-flow profiles, where the frequencies of these modes are incommensurate. Such profiles arise in experiments, e.g., Refs. 14 and 15. A perturbation consisting of both modes is quasi-periodic in time and space. Such a perturbation is more general and representative of reality but has not been considered using either the nonlinear critical-layer theory or the nonlinear parabolized stability equation (NPSE) approach.[40] The nonlinear interaction and evolution of such a form of disturbances are treated by introducing the phase variables, defined as the streamwise coordinate moving with the common phase speed multiplied by the wavenumbers of the modes. It should be pointed out that this work is pertinent only to wakes or jets that are convectively unstable and act as a "noise amplifier." Absolute instability may arise in certain wake flows, in which case a different theoretical perspective is needed, and the reader is referred to Refs. 41 and 42.

In Sec. II, the governing equations of the flow are presented, and the appropriate form of the disturbance is discussed. The asymptotic expansions of the outer and inner solutions are shown, and the leading-order terms in each expansion are derived. The two solutions are matched to give the nonlinear evolution system. In Sec. III, the resulting system is simplified through the introduction of normalized variables. The upstream and boundary conditions are deduced. In Sec. IV, we describe the numerical methods for solving the eigenvalue problem and the evolution system. A flow profile and the related parameters are selected for calculation, and the numerical results are presented and discussed. In Sec. V, a summary is given, and possible avenues for future work are highlighted.

II. FORMULATION

We consider an incompressible free shear flow that may be a wake or a jet. The steady base flow is subject to a 2D small-amplitude perturbation. The flow is to be described by the Cartesian coordinate system (x, y), where the streamwise and transverse coordinates, x and y, are both non-dimensionalized by using L_0, which is the characteristic wake or jet half-width. The x-axis, $y = 0$, coincides with the symmetry line of the base flow. The time t, velocity (u, v), and pressure p are made non-dimensional by L_0/U^*, U^*, and ρU^{*2}, respectively, where U^* is the characteristic velocity (which is taken to be the free-steam velocity U_∞ in the case of a plane wake or in the case of a jet, the maximum velocity as the location of interest), and ρ is the fluid density. The Reynolds number is defined as

$$R = L_0 U^* / \nu, \tag{1}$$

where ν is the kinematic viscosity of the fluid. As in Refs. 32, 33, and 37, the assumption that $R \gg 1$ is made here so that it is possible to develop a self-consistent asymptotic description of the nonlinear evolution of perturbation.

The total flow field can be written as

$$(u, v, p) = (\bar{U}(x^\dagger, y), R^{-1}\bar{V}(x^\dagger, y, P)) + (\tilde{u}, \tilde{v}, \tilde{p}), \tag{2}$$

where $x^\dagger = x/R$ describes the slow streamwise variation of the base flow and $(\tilde{u}, \tilde{v}, \tilde{p})$ is the perturbation flow field. The base flow is taken to be laminar, and the perturbation is assumed to be purely deterministic here. A possible adaptation of the theory to coherent structures in turbulent flows will be discussed at the end of this paper.

Substitution of Eq. (2) into the Navier–Stokes equations yields the equations for perturbation. Introducing the perturbation streamfunction ψ such that $\tilde{u} = \psi_y$ and $\tilde{v} = -\psi_x$, and eliminating the pressure $\tilde{p}$, the governing equations of the perturbation can be written as[38]

$$\left(\frac{\partial}{\partial t} + \bar{U}\frac{\partial}{\partial x}\right)\nabla^2\psi - \bar{U}''\frac{\partial\psi}{\partial x} - \frac{1}{R}\nabla^4\psi = \frac{\partial\psi}{\partial x}\frac{\partial\nabla^2\psi}{\partial y} - \frac{\partial\psi}{\partial y}\frac{\partial\nabla^2\psi}{\partial x}, \tag{3}$$

and note that the terms representing the non-parallel-flow effect have been neglected as they do not come into play to the order of interest.

In the natural condition without controlled excitation, the broadband spectra of both sinuous and varicose modes may amplify. Modes with different frequencies will become neutrally stable at different streamwise locations, where they nearly attain their maximum amplitudes through the accumulated linear growth, and the self-nonlinear interaction takes place in the critical layer, influencing the evolution.[32–34] For each sinuous mode, there is a

Published under license by AIP Publishing

corresponding varicose mode of a suitable frequency that becomes neutrally stable at the same streamwise location $x_0^\dagger$, close to which the two modes have the same phase speed c and thus share the two critical layers, which must coincide with the inflection points of the base-flow velocity profile.[43,44] Within the common critical layers, mutual interactions take place in addition to the respective self-interactions. Our focus is on the nonlinear dynamics of such a pair of interacting sinuous and varicose modes. These types of interactions can certainly be created by controlled excitation but are probably preferred in the natural condition in the presence of low-level free-stream disturbances because interactions of sinuous–sinuous and sinuous–varicose modes that do not have common critical layers are less effective.

Based on the above considerations, the leading-order perturbation in the main part of the wake or jet is taken to be a sum of the interacting sinuous and varicose modes. Both modes are initially described by linear stability theory, growing exponentially and then becoming neutral at the same downstream location $x_0^\dagger$.

As was shown for the mixing layer,[32,37] the nonlinear stage commences in a region that is upstream of the neutral position, $x_0^\dagger$, by a distance of $O(\varepsilon^{1/2}x_0^\dagger)$, where ε represents the amplitude of the modes. The normalized frequencies ω_s and ω_v of the two modes differ from their respective local neutral frequencies $\alpha_s c$ and $\alpha_v c$, respectively, by $O(\varepsilon^{1/2})$. Thus, ω_s and ω_v are written as

$$\omega_s = \alpha_s c + \varepsilon^{1/2}\Delta_s, \quad \omega_v = \alpha_v c + \varepsilon^{1/2}\Delta_v, \tag{4}$$

where Δ_s and Δ_v measure the scaled frequency deviations and α is the wavenumber of each mode. Variables pertaining to the sinuous and varicose modes are indicated by subscripts s and v, respectively. The modes evolve nonlinearly on the length scale of $O(\varepsilon^{-1/2})$ and can hence be described by the slow variable

$$x_1 = \varepsilon^{1/2}c^{-1}x, \tag{5}$$

where the factor c^{-1} is inserted for convenience. In order to include a possible temporal modulation, the slow time variable,

$$t_1 = \varepsilon^{1/2}t, \tag{6}$$

is introduced as in Ref. 38. The leading-order perturbation to the main part of the wake or jet can be written as $\psi = \varepsilon\psi_1$, with

$$\begin{aligned}\psi_1(x_1,t_1,x,y,t) = {} & A_v(x_1,t_1)\phi_{1v}(y)e^{i\alpha_v\xi} \\ & + A_s(x_1,t_1)\phi_{1s}(y)e^{i\alpha_s\xi} + c.c.,\end{aligned} \tag{7}$$

where A denotes the amplitude of each mode that is dependent on the slow variables x_1 and t_1, and ϕ_1 represents the eigenfunction. Here, we have introduced a coordinate traveling with the phase speed of the neutral modes, $\xi = x - ct$.

We are interested in the most general case where strong nonlinearity, non-equilibrium, and viscosity all appear at leading order in the critical layer. This occurs if $\varepsilon = O(R^{-2/3})$, and hence, R is scaled as[33]

$$R^{-1} = \lambda\varepsilon^{3/2}, \tag{8}$$

where $\lambda = O(1)$ is the Haberman parameter.[45] The previous study[37] considered the inviscid limit corresponding to $\lambda = 0$.

A. Perturbation outside of the critical layers

As in Refs. 32 and 37, the solution for the perturbation in the main part of the flow is sought in the form of asymptotic series,

$$\psi = \varepsilon\psi_1 + \varepsilon^{3/2}\psi_{3/2} + O(\varepsilon^2), \tag{9}$$

where the leading-order term ψ_1 is given by Eq. (7), while the higher-order term in ε, $\psi_{3/2}$, takes the following form:

$$\begin{aligned}\psi_{3/2}(x_1,t_1,\xi,y) &= \sum_{m,n}\phi_{3/2}^{(m,n)}(x_1,t_1,y)e^{i(m\alpha_s+n\alpha_v)\xi} \\ &= \sum_{m,n}\phi_{3/2}^{(m,n)}(x_1,t_1,y)e^{i(m\theta_s+n\theta_v)}.\end{aligned} \tag{10}$$

In general, α_s and α_v are incommensurable, that is, α_s/α_v is an irrational number, and hence, the solution is quasi-periodic. In Eq. (10), we have introduced the two phase variables

$$\theta_s = \alpha_s\xi, \quad \theta_v = \alpha_v\xi, \tag{11}$$

which can be treated as independent,[46] that is, $\psi_{3/2}$ is a quasi-periodic function of θ_s and θ_v, defined on a two-dimensional torus $\mathbb{T}^2 = [0, 2\pi] \times [0, 2\pi]$. This is significantly different from the Bickley jet for which $\alpha_s/\alpha_v = 2$ and the solution can be expressed as a usual Fourier series of a single variable.[37]

Substitution of Eqs. (7) and (9) into Eq. (3) and retaining the terms of $O(\varepsilon)$ give the equations for the eigenfunctions ϕ_{1s} and ϕ_{1v},

$$\mathscr{L}(\alpha_s)\phi_{1s} = 0, \quad \phi_{1s} \to 0 \text{ as } y \to \pm\infty, \quad \phi_{1s}(y) = \phi_{1s}(-y), \tag{12}$$

$$\mathscr{L}(\alpha_v)\phi_{1v} = 0, \quad \phi_{1s} \to 0 \text{ as } y \to \pm\infty, \quad \phi_{1v}(y) = -\phi_{1v}(-y), \tag{13}$$

where $\mathscr{L}(\alpha)$ is the Rayleigh operator,

$$\mathscr{L}(\alpha) = \left(\frac{\partial^2}{\partial y^2} - \alpha^2\right) - \frac{\bar{U}''}{\bar{U}-c}. \tag{14}$$

Note that the modes are distinguished by their symmetries with respect to y. The upper/lower critical levels, $\pm y_c$, appear at $U(\pm y_c) = c$, and they correspond to the inflection points, that is,

$$\bar{U}_c'' \equiv \bar{U}_{yy}(\pm y_c) = 0, \tag{15}$$

where the subscript c indicates the value of the quantity evaluated at a critical level. The result (15) was established in Refs. 43 and 44 by considering the Reynolds stress of the disturbance.

Equations (12) and (13) are known to have two linearly independent solutions, $\phi_a(y)$ and $\phi_b(y)$. For $\eta_\pm \equiv y \mp y_c \ll 1$, these can be constructed in the form of the Frobenius series,

$$\phi_a(\eta_\pm;\alpha) = \eta_\pm + \frac{1}{6}\left(\alpha^2 + \frac{\bar{U}_{c_\pm}'''}{\bar{U}_{c_\pm}'}\right)\eta_\pm^3 + \dots, \tag{16}$$

$$\phi_b(\eta_\pm;\alpha) = 1 + \frac{1}{2}\left(\alpha^2 + \frac{\bar{U}_{c_\pm}'''}{\bar{U}_{c_\pm}'}\right)\eta_\pm^2 + \frac{1}{12}\frac{\bar{U}_{c_\pm}^{iv}}{\bar{U}_{c_\pm}'}\eta_\pm^3 + \dots. \tag{17}$$

On imposing the respective symmetry conditions on the two modes, ϕ_{1s} and ϕ_{1v} can be written in the vicinity of each critical level as

$$\phi_{1s}(\eta_\pm) \sim \phi_b(\eta_\pm;\alpha_s) \pm a_s\phi_a(\eta_\pm;\alpha_s), \tag{18}$$

$$\phi_{1v}(\eta_\pm) \sim \pm\phi_b(\eta_\pm;\alpha_v) + a_v\phi_a(\eta_\pm;\alpha_v), \tag{19}$$

Published under license by AIP Publishing

where a_s and a_v are constants that remain to be determined. Both eigenfunctions have been normalized such that $\phi_{1s} = \phi_{1v} = 1$ at $y = y_c$. As $y \to \pm\infty$,

$$\phi_{1s}(y) \sim r_{s\infty} e^{-\alpha_s|y|} \quad , \quad \phi_{1v}(y) \sim \pm r_{v\infty} e^{-\alpha_v|y|}, \tag{20}$$

where $r_{s\infty}$ and $r_{v\infty}$ are constants.

Substituting Eqs. (7)–(10) into Eq. (3) and retaining the terms of $O(\varepsilon^{3/2})$, we obtain the equation for $\psi_{3/2}$ and hence the equations for $\phi_{3/2}^{(m,n)}$. As in Ref. 38, $\phi_{3/2}^{(1,0)}$ and $\phi_{3/2}^{(0,1)}$ obey the inhomogeneous Rayleigh equations,

$$\begin{aligned} \mathscr{L}(\alpha_s)\phi_{3/2}^{(1,0)} &= -\frac{2i\alpha_s}{c}\frac{\partial A_s}{\partial x}\phi_{1s} - (i\alpha_s)^{-1}\mathscr{D}_0 A_s \frac{\bar{U}''}{(\bar{U}-c)^2}\phi_{1s}, \\ \phi_{3/2}^{(1,0)} &\to 0 \ \text{ as } \ y \to \pm\infty, \end{aligned} \tag{21}$$

$$\begin{aligned} \mathscr{L}(\alpha_v)\phi_{3/2}^{(0,1)} &= -\frac{2i\alpha_v}{c}\frac{\partial A_v}{\partial x}\phi_{1v} - (i\alpha_v)^{-1}\mathscr{D}_0 A_v \frac{\bar{U}''}{(\bar{U}-c)^2}\phi_{1v}, \\ \phi_{3/2}^{(0,1)} &\to 0 \ \text{ as } \ y \to \pm\infty, \end{aligned} \tag{22}$$

where the differential operator $\mathscr{D}_0$ with respect to the slow variables is defined as

$$\mathscr{D}_0 = \frac{\partial}{\partial t_1} + \frac{\partial}{\partial x_1}. \tag{23}$$

By analyzing Eqs. (21) and (22) near to the upper and lower critical levels, the solutions for $\phi_{3/2}^{(1,0)}$ and $\phi_{3/2}^{(0,1)}$ are constructed in the form of the Frobenius series,

$$\begin{aligned} \phi_{3/2}^{(1,0)} \sim\ & b_{2s,\pm}\phi_b(\eta_\pm;\alpha_s) + a_{2s,\pm}^{\pm}\phi_a(\eta_\pm;\alpha_s) \\ & + \frac{i\bar{U}'''_{c_\pm}}{\alpha_s \bar{U}'^2_{c_\pm}}\mathscr{D}_0 A_s \eta_\pm \ln|\eta_\pm| \\ & + \left[-\frac{i\alpha_s}{c}\frac{\partial A_s}{\partial x_1} + \frac{1}{2}\frac{i\bar{U}'''_{c_\pm}\chi_{s\pm}}{\alpha_s \bar{U}'^2_{c_\pm}}\mathscr{D}_0 A_s\right]\eta_\pm^2 \\ & + O(\eta_\pm^3 \ln|\eta_\pm|), \end{aligned} \tag{24}$$

$$\begin{aligned} \phi_{3/2}^{(0,1)} \sim\ & b_{2v,\pm}\phi_b(\eta_\pm;\alpha_v) + a_{2v,\pm}^{\pm}\phi_a(\eta_\pm;\alpha_v)s \\ & \pm \frac{i\bar{U}'''_{c_\pm}}{\alpha_v \bar{U}'^2_{c_\pm}}\mathscr{D}_0 A_v \eta_\pm \ln|\eta_\pm| \\ & \pm \left[-\frac{i\alpha_v}{c}\frac{\partial A_v}{\partial x_1} + \frac{1}{2}\frac{i\bar{U}'''_{c_\pm}\chi_{v\pm}}{\alpha_v \bar{U}'^2_{c_\pm}}\mathscr{D}_0 A_v\right]\eta_\pm^2 \\ & + O(\eta_\pm^3 \ln|\eta_\pm|), \end{aligned} \tag{25}$$

where $a_{2s,\pm}^{\pm}$, $a_{2v,\pm}^{\pm}$, $b_{2s,\pm}$, and $b_{2v,\pm}$ are all functions of the slow variables x_1 and t_1, with $a_{2s,\pm}^{+}$ and $a_{2s,\pm}^{-}$ corresponding to the values above and below each critical layer, respectively. The jumps in their values occur due to the presence of the $\ln|\eta_\pm|$ term in solutions (24) and (25) and will be determined by analyzing the dynamics in the critical layers. For brevity, we have put $\chi_{s\pm} = \pm a_{1s} + \frac{1}{2}\frac{\bar{U}_c^{iv}}{\bar{U}_c'''}$ and $\chi_{v\pm} = \pm a_{1v} + \frac{1}{2}\frac{\bar{U}_c^{iv}}{\bar{U}_c'''}$. In order for Eqs. (21) and (22) to have solutions satisfying the boundary conditions, the solvability conditions,

$$\begin{aligned} & (a_{2s,+}^{+} - a_{2s,+}^{-}) + (a_{2s,-}^{+} - a_{2s,-}^{-}) \\ & \quad = -i\alpha_s^{-1} J_{2s}\frac{\partial A_s}{\partial t_1} + i[2\alpha_s c^{-1} J_{1s} - \alpha_s^{-1} J_{2s}]\frac{\partial A_s}{\partial x_1} \end{aligned} \tag{26}$$

and

$$\begin{aligned} & (a_{2v,+}^{+} - a_{2v,+}^{-}) - (a_{2v,-}^{+} - a_{2v,-}^{-}) \\ & \quad = -i\alpha_v^{-1} J_{2v}\frac{\partial A_v}{\partial t_1} + i[2\alpha_v c^{-1} J_{1v} - \alpha_v^{-1} J_{2v}]\frac{\partial A_v}{\partial x_1}, \end{aligned} \tag{27}$$

have to be satisfied,[37,38,47] where

$$J_{1s} = \int_{-\infty}^{\infty} \phi_{1s}^2 \mathrm{d}y, \quad J_{2s} = \fint_{-\infty}^{\infty} \frac{\bar{U}''\phi_{1s}^2}{(\bar{U}-c)^2}\mathrm{d}y, \tag{28}$$

and J_{1v} and J_{2v} have the same expressions as J_{1s} and J_{2s}, respectively, provided that ϕ_{1s} is replaced by ϕ_{1v}. Equations (26) and (27) are derived by first multiplying Eqs. (21) and (22) by ϕ_{1s} and ϕ_{1v}, respectively.[33,37] The left-hand sides are then integrated by parts using the asymptotic expansions (24) and (25) at either side of both critical layers to account for the jumps. Specifically, the logarithmic terms of the form $\ln|y \pm y_c|$ on the left- and right-hand sides of the equations cancel out, which implies that the integrals J_{2s} and J_{2v} should be interpreted as Cauchy principal values. In the strictly linear regime, the jumps $(a_{2s,\pm}^{+} - a_{2s,\pm}^{-})$ and $(a_{2v,\pm}^{+} - a_{2v,\pm}^{-})$ correspond to the classical rule of a phase shift by $-\pi\mathrm{sign}\big(U'(\pm y_c)\big)$ across the critical layer, that is, $\ln(y \pm y_c)$ in Eqs. (24) and (25) takes the value $\ln|y \pm y_c| - \mathrm{sign}\big(U'(\pm y_c)\pi i$ when $y < \pm y_c$. This rule no longer holds when the critical-layer dynamics becomes nonlinear, and the jumps have to be determined by a detailed analysis of the respective critical layers. It is through these jumps that the nonlinear interactions in the thin critical layers influence the overall development of the modes.[34]

The harmonic components $\phi_{3/2}^{(m,n)}$ (where if $m = 0$, $n \neq 1$ and if $n = 0$, $m \neq 1$) obey the homogeneous Rayleigh equation,

$$\mathscr{L}(m\alpha_s + n\alpha_v)\phi_{3/2}^{(m,n)} = 0, \ \ \phi_{3/2}^{(m,n)} \to 0 \ \text{ as } \ y \to \pm\infty, \tag{29}$$

and so in the vicinity of each critical level, $\phi_{3/2}^{(m,n)}$ has the local solution,

$$\begin{aligned} \phi_{3/2}^{(m,n)}(x_1, t_1, \eta_\pm) \sim\ & b_{2,\pm}^{(m,n)}\left[1 + \frac{1}{2}\left((m\alpha_s + n\alpha_v)^2 + \frac{\bar{U}'''_{c_\pm}}{\bar{U}'_{c_\pm}}\right)\eta_\pm^2\right] \\ & + a_{2,\pm}^{(m,n),\pm}\eta_\pm + O(\eta_\pm^2). \end{aligned} \tag{30}$$

Despite the harmonic components obeying the homogeneous Rayleigh equation, they do not constitute eigenfunctions because there is, as will be shown later, a forcing from within the critical layers through the two jumps, $(a_{2,+}^{(m,n),+} - a_{2,+}^{(m,n),-})$ and $(a_{2,-}^{(m,n),+} - a_{2,-}^{(m,n),-})$, for each mode.

B. Perturbation inside the critical layers

In order to obtain the jumps $(a_{2s,\pm}^{+} - a_{2s,\pm}^{-})$, $(a_{2v,\pm}^{+} - a_{2v,\pm}^{-})$, and $(a_{2,\pm}^{(m,n),+} - a_{2,\pm}^{(m,n),-})$, we have to analyze the perturbations inside the critical layers. As the strongly nonlinear critical layers have an

Published under license by AIP Publishing

$O(\varepsilon^{1/2})$ thickness,[32,48] the local transverse variable for each critical layer is taken to be

$$Y_\pm = (y \mp y_c)/\varepsilon^{1/2} = \eta_\pm/\varepsilon^{1/2}, \tag{31}$$

and the streamfunction is expanded as[32,38]

$$\psi^\pm = \varepsilon\Psi_1^\pm + \varepsilon^{3/2}\Psi_{3/2}^\pm + \varepsilon^2 \ln \varepsilon^{1/2}\Psi_{2L}^\pm + \varepsilon^2\Psi_2^\pm + \dots . \tag{32}$$

The solutions for $\Psi_1^\pm$, $\Psi_{3/2}^\pm$, and $\Psi_{2L}^\pm$ that match with their outer counterparts are

$$\Psi_1^\pm(x_1, t_1, Y_\pm, \xi) = A_s e^{i\alpha_s\xi} \pm A_v e^{i\alpha_v\xi} + \text{c.c.}, \tag{33}$$

$$\Psi_{3/2}^\pm(x_1, t_1, Y_\pm, \xi) = \sum_{m,n} b_{2,\pm}^{(m,n)} e^{i(m\alpha_s + n\alpha_v)\xi} + a_{1v} Y_\pm A_v e^{i\alpha_v\xi} \pm a_{1s} Y_\pm A_s e^{i\alpha_s\xi} + \text{c.c.}, \tag{34}$$

$$\Psi_{2L}^\pm(x_1, t_1, Y_\pm, \xi) = \frac{i\bar{U}_{c_\pm}'''}{\alpha_s \bar{U}_{c_\pm}'^2} \mathscr{D}_0 A_s Y_\pm e^{i\alpha_s\xi} \pm \frac{i\bar{U}_{c_\pm}'''}{\alpha_v \bar{U}_{c_\pm}'^2} \mathscr{D}_0 A_v Y_\pm e^{i\alpha_v\xi} + \text{c.c.} \tag{35}$$

Following the procedure in Refs. 32 and 37 to obtain an expression for $\Psi_2^\pm$, we introduce the variable

$$\Omega^\pm = \frac{\partial^2\Psi_2^\pm}{\partial Y_\pm^2} - \left(\alpha_s^2 + \frac{\bar{U}_{c_\pm}'''}{\bar{U}_{c_\pm}'}\right) A_s e^{i\alpha_s\xi} \mp \left(\alpha_v^2 + \frac{\bar{U}_{c_\pm}'''}{\bar{U}_{c_\pm}'}\right) A_v e^{i\alpha_v\xi} + c.c. \tag{36}$$

Substituting Eq. (32) into Eq. (3) and using Eqs. (33)–(36), relation (8), and the scalings of x_1, t_1, and $Y_\pm$, we find that $\Omega^\pm$ is governed by the equation

$$\mathscr{L}_{\mathscr{N}}^\pm \Omega^\pm = -\frac{\bar{U}_{c_\pm}'''}{\bar{U}_{c_\pm}'} \mathscr{D}_0 \left(A_s e^{i\alpha_s\xi} \pm A_v e^{i\alpha_v\xi}\right) + c.c., \tag{37}$$

where

$$\mathscr{L}_{\mathscr{N}}^\pm = \left(\mathscr{D}_0 + \bar{U}_{c_\pm}' Y_\pm \frac{\partial}{\partial\xi}\right) - \lambda\frac{\partial^2}{\partial Y_\pm^2} - i\left(\alpha_s A_s e^{i\alpha_s\xi} \pm \alpha_v A_v e^{i\alpha_v\xi} - c.c.\right)\frac{\partial}{\partial Y_\pm}. \tag{38}$$

The solution for $\Omega^\pm$ can be expressed as

$$\Omega^\pm(x_1, t_1, Y_\pm, \xi) = \sum_{m,n=-\infty}^{\infty} Q_{m,n}^\pm(x_1, t_1, Y_\pm) e^{i(m\alpha_s\xi + n\alpha_v\xi)} = \sum_{m,n=-\infty}^{\infty} Q_{m,n}^\pm(x_1, t_1, Y_\pm) e^{i(m\theta_s + n\theta_v)}. \tag{39}$$

Similar to $\psi_{3/2}$ given by Eq. (10), $\Omega^\pm$ is a quasi-periodic function for an irrational ratio α_s/α_v and is expressed as a function of the phase variables θ_s and θ_v.[46] Substitution of Eq. (39) into Eq. (37) gives the equations for $Q_{m,n}^\pm$,

$$\begin{aligned}\left[\mathscr{D}_0 + i\bar{U}_{c_\pm}' Y_\pm(\alpha_s m + \alpha_v n) - \lambda\frac{\partial^2}{\partial Y_\pm^2}\right] Q_{m,n}^\pm &- i\left[\alpha_s A_s \frac{\partial Q_{m-1,n}^\pm}{\partial Y_\pm} \pm \alpha_v A_v \frac{\partial Q_{m,n-1}^\pm}{\partial Y_\pm} - \left(\alpha_s A_s^* \frac{\partial Q_{m+1,n}^\pm}{\partial Y_\pm} \pm \alpha_v A_v^* \frac{\partial Q_{m,n+1}^\pm}{\partial Y_\pm}\right)\right] \\ &= -\frac{\bar{U}_{c_\pm}'''}{\bar{U}_{c_\pm}'} \mathscr{D}_0 \left(\delta_{m,1}\delta_{0,n} A_s \pm \delta_{m,0}\delta_{1,n} A_v + \delta_{m,-1}\delta_{0,n} A_s^* \pm \delta_{m,0}\delta_{-1,n} A_v^*\right),\end{aligned} \tag{40}$$

where * denotes a complex conjugate. The velocity jumps in the Fourier components can be calculated by integrating $\Omega^\pm$ with respect to θ_s and θ_v (for all m, n). Equating the jumps with those in the outer solution (30) for the non-fundamental components, we obtain

$$\frac{1}{(2\pi)^2}\int_0^{2\pi}\int_0^{2\pi}\int_{-\infty}^{\infty} \Omega^+ e^{-im\theta_s - in\theta_v} \mathrm{d}Y_+ \mathrm{d}\theta_s \mathrm{d}\theta_v = \int_{-\infty}^{\infty} Q_{m,n}^+ \mathrm{d}Y_+ = a_{2,+}^{(m,n),+} - a_{2,+}^{(m,n),-}, \tag{41}$$

$$\frac{1}{(2\pi)^2}\int_0^{2\pi}\int_0^{2\pi}\int_{-\infty}^{\infty} \Omega^- e^{-im\theta_s - in\theta_v} \mathrm{d}Y_- \mathrm{d}\theta_s \mathrm{d}\theta_v = \int_{-\infty}^{\infty} Q_{m,n}^- \mathrm{d}Y_- = a_{2,-}^{(m,n),+} - a_{2,-}^{(m,n),-}. \tag{42}$$

Equating the jumps with those in the outer solutions (24) and (25) for the fundamental sinuous ($m = 1$, $n = 0$) and varicose modes ($m = 0$, $n = 1$), respectively, and making use of Eqs. (26) and (27) for the fundamental sinuous ($m = 1$, $n = 0$) and varicose ($m = 0$, $n = 1$) modes, respectively, we arrive at the following relations:

$$\int_{-\infty}^{\infty} Q_{1,0}^+ \mathrm{d}Y_+ + \int_{-\infty}^{\infty} Q_{1,0}^- \mathrm{d}Y_- = -i\alpha_s^{-1} J_{2s}\frac{\partial A_s}{\partial t_1} + i\left[2\alpha_s c^{-1} J_{1s} - \alpha_s^{-1} J_{2s}\right]\frac{\partial A_s}{\partial x_1}, \tag{43}$$

$$\int_{-\infty}^{\infty} Q_{0,1}^+ \mathrm{d}Y_+ - \int_{-\infty}^{\infty} Q_{0,1}^- \mathrm{d}Y_- = -i\alpha_v^{-1} J_{2v}\frac{\partial A_v}{\partial t_1} + i\left[2\alpha_v c^{-1} J_{1v} - \alpha_v^{-1} J_{2v}\right]\frac{\partial A_v}{\partial x_1}. \tag{44}$$

Equations (40), (43), and (44) govern the nonlinear evolution of the interacting sinuous and varicose modes.

By introducing the slow time variable t_1 [see Eq. (6)], the present theory can describe the interactions among side-band components in narrow bands centered at ω_s and ω_v. However, a mathematical description of interactions among a broadband of modes remains a challenging and largely open problem (see Ref. 49 for a discussion), and we shall return to this issue at the end of this paper.

Published under license by AIP Publishing

III. COUPLED EVOLUTION SYSTEM

Equations (40), (43), and (44) can be simplified somewhat by introducing the renormalized dependent variables

$$\tilde{A}_s = \bar{U}'_{c_+} A_s, \quad \tilde{A}_v = \bar{U}'_{c_+} A_v, \quad \tilde{Q}^{\pm}_{mn} = Q^{\pm}_{mn} (\bar{U}'_{c_\pm})^2 / \bar{U}'''_{c_\pm}, \tag{45}$$

the independent variable

$$\tilde{\eta}_\pm = \bar{U}'_{c_\pm} Y_\pm, \tag{46}$$

and the parameter

$$\tilde{\lambda} = (\bar{U}'_{c_\pm})^2 \lambda. \tag{47}$$

Noting that $\bar{U}'_{c_+} = -\bar{U}'_{c_-}$ and $\bar{U}'''_{c_+} = -\bar{U}'''_{c_-}$, Eq. (40) can be rewritten as

$$\begin{aligned}
&\left[\mathscr{D}_0 + i\tilde{\eta}_\pm(\alpha_s m + \alpha_v n) - \tilde{\lambda}\frac{\partial^2}{\partial \tilde{\eta}_\pm^2}\right]\tilde{Q}^{\pm}_{m,n} \\
&\quad + i\left[\alpha_v \tilde{A}_v^* \frac{\partial \tilde{Q}^{\pm}_{m,n+1}}{\partial \tilde{\eta}_\pm} \pm \alpha_s \tilde{A}_s^* \frac{\partial \tilde{Q}^{\pm}_{m+1,n}}{\partial \tilde{\eta}_\pm}\right. \\
&\quad \left. - \left(\alpha_v \tilde{A}_v \frac{\partial \tilde{Q}^{\pm}_{m,n-1}}{\partial \tilde{\eta}_\pm} \pm \alpha_s \tilde{A}_s \frac{\partial \tilde{Q}^{\pm}_{m-1,n}}{\partial \tilde{\eta}_\pm}\right)\right] \\
&= -\mathscr{D}_0\big(\pm\delta_{m,1}\delta_{0,n}\tilde{A}_s + \delta_{m,0}\delta_{1,n}\tilde{A}_v \\
&\quad \pm \delta_{m,-1}\delta_{0,n}\tilde{A}_s^* + \delta_{m,0}\delta_{-1,n}\tilde{A}_v^*\big),
\end{aligned} \tag{48}$$

while the jump conditions [Eqs. (43) and (44)] become

$$\int_{-\infty}^{\infty} \tilde{Q}^{+}_{1,0} \mathrm{d}\tilde{\eta}_+ - \int_{-\infty}^{\infty} \tilde{Q}^{-}_{1,0} \mathrm{d}\tilde{\eta}_- = \Lambda_{1s}\frac{\partial \tilde{A}_s}{\partial t_1} + \Lambda_{2s}\frac{\partial \tilde{A}_s}{\partial x_1}, \tag{49}$$

$$\int_{-\infty}^{\infty} \tilde{Q}^{+}_{0,1} \mathrm{d}\tilde{\eta}_+ + \int_{-\infty}^{\infty} \tilde{Q}^{-}_{0,1} \mathrm{d}\tilde{\eta}_- = \Lambda_{1v}\frac{\partial \tilde{A}_v}{\partial t_1} + \Lambda_{2v}\frac{\partial \tilde{A}_v}{\partial x_1}, \tag{50}$$

where we have put

$$\Lambda_{1s} = -\frac{i\bar{U}'^2_{c_+}}{\alpha_s \bar{U}'''_{c_+}} J_{2s}, \quad \Lambda_{2s} = \frac{i\bar{U}'^2_{c_+}}{\bar{U}'''_{c_+}}[2\alpha_s c^{-1} J_{1s} - \alpha_s^{-1} J_{2s}], \tag{51}$$

$$\Lambda_{1v} = -\frac{i\bar{U}'^2_{c_+}}{\alpha_v \bar{U}'''_{c_+}} J_{2v}, \quad \Lambda_{2v} = \frac{i\bar{U}'^2_{c_+}}{\bar{U}'''_{c_+}}[2\alpha_v c^{-1} J_{1v} - \alpha_v^{-1} J_{2v}]. \tag{52}$$

In order to solve the rescaled evolution equations (48)–(50), first it is necessary to specify the appropriate initial (upstream) and boundary (far field) conditions, which we will derive next.

A. Upstream condition

The initial conditions can be derived by considering the behaviors of the disturbance in the upstream limit ($x_1 \to -\infty$). Since the disturbance is exponentially small there, the nonlinear terms in Eq. (48) can be neglected. The resulting linear equation is then solved to obtain

$$\tilde{Q}^{\pm}_{1,0} = \tilde{Q}^{\pm\star}_{-1,0} = \mp\int_0^{\infty} \mathscr{D}_0 \tilde{A}_s(x_1 - \zeta, t_1 - \zeta) e^{-\frac{1}{3}\tilde{\lambda}\alpha_s^2\zeta^3 - i\alpha_s\zeta\tilde{\eta}_\pm} \mathrm{d}\zeta, \tag{53}$$

$$\tilde{Q}^{\pm}_{0,1} = \tilde{Q}^{\pm\star}_{0,-1} = -\int_0^{\infty} \mathscr{D}_0 \tilde{A}_v(x_1 - \zeta, t_1 - \zeta) e^{-\frac{1}{3}\tilde{\lambda}\alpha_v^2\zeta^3 - i\alpha_v\zeta\tilde{\eta}_\pm} \mathrm{d}\zeta, \tag{54}$$

with all other $Q^{\pm}_{m,n}$ terms being equal to 0. Integration of both sides with respect to $\eta_\pm$ gives

$$\int_{-\infty}^{\infty} \tilde{Q}^{\pm}_{1,0} \mathrm{d}\eta_\pm = \mp\pi\mathscr{D}_0\tilde{A}_s, \quad \int_{-\infty}^{\infty} \tilde{Q}^{\pm}_{0,1} \mathrm{d}\eta_\pm = -\pi\mathscr{D}_0\tilde{A}_v, \tag{55}$$

which are then substituted into Eqs. (49) and (50) to give the equations governing $\tilde{A}_s$ and $\tilde{A}_v$ upstream as

$$\frac{\partial \tilde{A}_s}{\partial t_1} + c_s\frac{\partial \tilde{A}_s}{\partial x_1} = 0, \quad \frac{\partial \tilde{A}_v}{\partial t_1} + c_v\frac{\partial \tilde{A}_v}{\partial x_1} = 0, \tag{56}$$

where

$$c_s = 1 - 2\alpha_s^2 c^{-1} J_{1s} \Big/ \left(\frac{2i\pi\bar{U}'''_{c_+}}{\bar{U}'^2_{c_+}} + J_{2s}\right), \tag{57}$$

$$c_v = 1 - 2\alpha_v^2 c^{-1} J_{1v} \Big/ \left(\frac{2i\pi\bar{U}'''_{c_+}}{\bar{U}'^2_{c_+}} + J_{2v}\right) \tag{58}$$

are the group velocities. Due to the group velocities being complex numbers for $u_0 = O(1)$, a coordinate moving with the group velocity cannot be defined.[38,47] This means that the modulation equations have to be of first order rather than second order as they would be if c_s and c_v were real numbers.

B. Boundary conditions

The boundary conditions on $Q^{\pm}_{m,n}$ are obtained by considering the limiting behavior of Eq. (48) as $\tilde{\eta}_\pm \to \pm\infty$. The dominant balance gives

$$\tilde{Q}^{\pm}_{1,0} = \tilde{Q}^{\pm*}_{-1,0} \to \pm\left(\frac{i}{\tilde{\eta}_\pm\alpha_s} - \frac{\mathscr{D}_0}{\tilde{\eta}_\pm^2\alpha_s^2} - \frac{i\mathscr{D}_0^2}{\tilde{\eta}_\pm^3\alpha_s^3}\right)\mathscr{D}_0\tilde{A}_s + O(\tilde{\eta}_\pm^{-4}), \tag{59}$$

$$\tilde{Q}^{\pm}_{0,1} = \tilde{Q}^{\pm*}_{0,-1} \to \left(\frac{i}{\tilde{\eta}_\pm\alpha_v} - \frac{\mathscr{D}_0}{\tilde{\eta}_\pm^2\alpha_v^2} - \frac{i\mathscr{D}_0^2}{\tilde{\eta}_\pm^3\alpha_v^3}\right)\mathscr{D}_0\tilde{A}_v + O(\tilde{\eta}_\pm^{-4}), \tag{60}$$

$$\begin{aligned}
\tilde{Q}^{\pm}_{0,0} \to &-\frac{1}{\tilde{\eta}_\pm^2}\left(|A_s|^2 + |A_v|^2\right) \\
&+ \frac{2i}{\tilde{\eta}_\pm^3}\left(\frac{\tilde{A}_s\mathscr{D}_0\tilde{A}_s^* - c.c.}{\alpha_s} + \frac{\tilde{A}_v\mathscr{D}_0\tilde{A}_v^* - c.c.}{\alpha_v}\right) + O(\tilde{\eta}_\pm^{-4}),
\end{aligned} \tag{61}$$

$$\begin{aligned}
\tilde{Q}^{\pm}_{1,1} = \tilde{Q}^{\pm*}_{-1,-1} \to &\mp\frac{i}{(\alpha_s + \alpha_v)\tilde{\eta}_\pm^3}\left(\frac{\alpha_s}{\alpha_v}\tilde{A}_s\mathscr{D}_0\tilde{A}_v + \frac{\alpha_v}{\alpha_s}\tilde{A}_v\mathscr{D}_0\tilde{A}_s\right) \\
&+ O(\tilde{\eta}_\pm^{-4}),
\end{aligned} \tag{62}$$

$$\tilde{Q}^{\pm}_{2,0} = \tilde{Q}^{\pm^*}_{-2,0} \to -\frac{i}{2\alpha_s\tilde{\eta}_\pm^3}\left(\tilde{A}_s\mathscr{D}_0\tilde{A}_s\right) + O(\tilde{\eta}_\pm^{-4}), \tag{63}$$

$$\tilde{Q}^{\pm}_{0,2} = \tilde{Q}^{\pm*}_{0,-2} \to -\frac{i}{2\alpha_v\tilde{\eta}_\pm^3}\left(\tilde{A}_v\mathscr{D}_0\tilde{A}_v\right) + O(\tilde{\eta}_\pm^{-4}), \tag{64}$$

$$\begin{aligned}
\tilde{Q}^{\pm}_{1,-1} = \tilde{Q}^{\pm^*}_{-1,1} \to &\pm\frac{i}{(\alpha_s - \alpha_v)\tilde{\eta}_\pm^3}\left(\frac{\alpha_s}{\alpha_v}\tilde{A}_s\mathscr{D}_0\tilde{A}_v^* + \frac{\alpha_v}{\alpha_s}\tilde{A}_v^*\mathscr{D}_0\tilde{A}_s\right) \\
&+ O(\tilde{\eta}_\pm^{-4}).
\end{aligned} \tag{65}$$

All other $\tilde{Q}^{\pm}_{m,n}$ terms decay like $O(\tilde{\eta}_\pm^{-4})$ or faster.

Published under license by AIP Publishing

C. Truncating the integrals in the evolution equations

The rescaled critical-layer vorticity equation (48) has to be solved, and the integrals in Eqs. (49) and (50) have to be evaluated numerically in a finite but large domain $-H \le \tilde{\eta}_\pm \le H$. After making use of the boundary conditions (59) and (60) to approximate the Cauchy principal value integration of the $1/\tilde{\eta}_\pm$ terms, Eqs. (49) and (50) become

$$\int_{-H}^{H} \tilde{Q}^{+}_{1,0}\mathrm{d}\tilde{\eta}_+ - \int_{-H}^{H} \tilde{Q}^{-}_{1,0}\mathrm{d}\tilde{\eta}_- - \frac{4\mathscr{D}_0^2\tilde{A}_s}{\alpha_s^2 H} + O(H^{-3}) = \Lambda_{1s}\frac{\partial \tilde{A}_s}{\partial t_1} + \Lambda_{2s}\frac{\partial \tilde{A}_s}{\partial x_1}, \tag{66}$$

$$\int_{-H}^{H} \tilde{Q}^{+}_{0,1}\mathrm{d}\tilde{\eta}_+ + \int_{-H}^{H} \tilde{Q}^{-}_{0,1}\mathrm{d}\tilde{\eta}_- - \frac{4\mathscr{D}_0^2\tilde{A}_v}{\alpha_v^2 H} + O(H^{-3}) = \Lambda_{1v}\frac{\partial \tilde{A}_v}{\partial t_1} + \Lambda_{2v}\frac{\partial \tilde{A}_v}{\partial x_1}. \tag{67}$$

The second-order derivative with respect to x_1 is difficult to discretize, and so a similar procedure to that in Ref. 38 is followed to convert Eqs. (66) and (67) to a first-order form,

$$\tilde{\Lambda}_{1s}\frac{\partial \tilde{A}_s}{\partial t_1} + \tilde{\Lambda}_{2s}\frac{\partial \tilde{A}_s}{\partial x_1} - \left(\tilde{\Lambda}_{d,1s}\frac{\partial^2}{\partial t_1^2} + \tilde{\Lambda}_{d,2s}\frac{\partial^2}{\partial x_1 \partial t_1}\right)\tilde{A}_s = \mathscr{D}_{1s} I_{0,1,0} + \frac{4iI_{1,1,0}}{\alpha_s H} - \frac{16}{\alpha_s^2 H^2 \Lambda_{2s}}\left(I_{2,1,0} - \tilde{A}_s^* I_{0,2,0}\right), \tag{68}$$

with $O(H^{-3})$ accuracy, where

$$\tilde{\Lambda}_{js} = \Lambda_{js}\left(\Lambda_{2s} - \frac{16}{\alpha_s^2\Lambda_{2s}}\right) - \frac{16}{\alpha_s^2} \quad (j = 1, 2), \tag{69}$$

$$\tilde{\Lambda}_{d,js} = \frac{4(\Lambda_{1s} - \Lambda_{2s})}{\alpha_s^2 H}\left(1 + \frac{\Lambda_{js}}{\Lambda_{2s}}\right) \quad (j = 1, 2). \tag{70}$$

The derivation is given in Appendix A. Application of the same procedure to Eq. (67) for the varicose mode leads to

$$\tilde{\Lambda}_{1v}\frac{\partial \tilde{A}_v}{\partial t_1} + \tilde{\Lambda}_{2v}\frac{\partial \tilde{A}_v}{\partial x_1} - \left(\tilde{\Lambda}_{d,1v}\frac{\partial^2}{\partial t_1^2} + \tilde{\Lambda}_{d,2v}\frac{\partial^2}{\partial x_1 \partial t_1}\right)\tilde{A}_v = \mathscr{D}_{1v} I_{0,0,1} + \frac{4iI_{1,0,1}}{\alpha_v H} - \frac{16}{\alpha_v^2 H^2 \Lambda_{2v}}\left(I_{2,0,1} - \tilde{A}_v^* I_{0,0,2}\right), \tag{71}$$

where

$$I_{k,0,n} = \int_{-H}^{H} \tilde{\eta}_+^k \tilde{Q}^{+}_{0,n}\mathrm{d}\tilde{\eta}_+ + \int_{-H}^{H} \tilde{\eta}_-^k \tilde{Q}^{-}_{0,0}\mathrm{d}\tilde{\eta}_-, \tag{72}$$

$$\tilde{\Lambda}_{jv} = \Lambda_{jv}\left(\Lambda_{2v} - \frac{16}{\alpha_v^3\Lambda_{2v}}\right) - \frac{16}{\alpha_v^2} \quad (j = 1, 2), \tag{73}$$

$$\tilde{\Lambda}_{d,jv} = \frac{4(\Lambda_{1v} - \Lambda_{2v})}{\alpha_v^2 H}\left(1 + \frac{\Lambda_{jv}}{\Lambda_{2v}}\right) \quad (j = 1, 2). \tag{74}$$

D. Interaction of sinuous and varicose modes

The formulation thus far allows the disturbance to be modulated slowly in time, that is, each mode may consist of a discrete set, or a continuum, of side-band components of the central frequency.[38]

Hereafter, the focus will be on the simpler case, where the side-band components are absent, i.e., only single sinuous and varicose modes are present. In this case, the dependence of $\tilde{A}_s$, $\tilde{A}_v$, and $\tilde{Q}_{m,n}$ on t_1 can be written as[33,37]

$$\tilde{A}_s(x_1, t_1) = \hat{A}_s(x_1)e^{-i\Delta_s t_1}, \quad \tilde{A}_v(x_1, t_1) = \hat{A}_v(x_1)e^{-i\Delta_v t_1}, \quad \tilde{Q}^{\pm}_{m,n}(x_1, t_1) = \hat{Q}^{\pm}_{m,n}(x_1)e^{-i(m\Delta_s + n\Delta_v)t_1}, \tag{75}$$

where Δ_s and Δ_v are the deviations of the frequencies of the sinuous and varicose modes from their respective neutral values, as Eq. (4) indicates. With the solution form (75), Eq. (48) becomes

$$\left[\frac{\partial}{\partial x_1} + i\tilde{\eta}_\pm(\alpha_s m + \alpha_v n) - i(\Delta_s m + \Delta_v n) - \tilde{\lambda}\frac{\partial^2}{\partial \tilde{\eta}_\pm^2}\right]\hat{Q}^{\pm}_{m,n} + i\left[\alpha_v\tilde{A}_v^*\frac{\partial \hat{Q}^{\pm}_{m,n+1}}{\partial \tilde{\eta}_\pm} \pm \alpha_s\tilde{A}_s^*\frac{\partial \hat{Q}^{\pm}_{m+1,n}}{\partial \tilde{\eta}_\pm} - \left(\alpha_v\tilde{A}_v\frac{\partial \hat{Q}^{\pm}_{m,n-1}}{\partial \tilde{\eta}_\pm} \pm \alpha_s\tilde{A}_s\frac{\partial \hat{Q}^{\pm}_{m-1,n}}{\partial \tilde{\eta}_\pm}\right)\right] = \mp\delta_{0,n}\left(\delta_{m,1}\mathscr{D}_s\tilde{A}_s + \delta_{m,-1}\mathscr{D}_s^*\tilde{A}_s^*\right) - \delta_{m,0}\left(\delta_{1,n}\mathscr{D}_v\tilde{A}_v + \delta_{-1,n}\mathscr{D}_v^*\tilde{A}_v^*\right), \tag{76}$$

where $\mathscr{D}_s = \frac{\partial}{\partial x_1} - i\Delta_s$ and $\mathscr{D}_v = \frac{\partial}{\partial x_1} - i\Delta_v$. Substitution of Eq. (75) into Eqs. (59)–(65) leads to the boundary conditions for $\hat{Q}^{\pm}_{m,n}$ ($m = 0, \pm1, \pm2$ and $n = 0, \pm1, \pm2$), which are given in Appendix B.

After substituting Eq. (75) into Eqs. (68) and (71), the governing equations for $\tilde{A}_s$ and $\tilde{A}_v$ are written as

$$(\tilde{\Lambda}_{2s} + i\Delta_s\tilde{\Lambda}_{d,2s})\frac{\partial \tilde{A}_s}{\partial x_1} + (\Delta_s^2\tilde{\Lambda}_{d,1s} - i\Delta_s\tilde{\Lambda}_{1s})\tilde{A}_s = \tilde{\mathscr{D}}_{1s}\tilde{I}_{0,1,0} + \frac{4i\tilde{I}_{1,1,0}}{\alpha_s^2 H} - \frac{16}{\alpha_s^3 H^2\Lambda_{2s}}\left(\tilde{I}_{2,1,0} - \tilde{A}_s^*\tilde{I}_{0,2,0}\right), \tag{77}$$

$$(\tilde{\Lambda}_{2v} + i\Delta_v\tilde{\Lambda}_{d,2v})\frac{\partial \tilde{A}_v}{\partial x_1} + (\Delta_v^2\tilde{\Lambda}_{d,1v} - i\Delta_v\tilde{\Lambda}_{1v})\tilde{A}_v = \tilde{\mathscr{D}}_{1v}\tilde{I}_{0,0,1} + \frac{4i\tilde{I}_{1,1,0}}{\alpha_v^2 H} - \frac{16}{\alpha_v^3 H^2\Lambda_{2v}}\left(\tilde{I}_{2,0,1} - \tilde{A}_v^*\tilde{I}_{0,0,2}\right), \tag{78}$$

where $\tilde{I}_{k,m,0}$ and $\tilde{I}_{k,0,n}$ have the same expressions as $I_{k,m,0}$ and $I_{k,0,n}$, provided that $Q^{\pm}_{m,0}$ and $Q^{\pm}_{0,n}$ are replaced by $\tilde{Q}^{\pm}_{m,0}$ and $\tilde{Q}^{\pm}_{0,n}$, respectively, and

$$\tilde{\mathscr{D}}_{1s} = \Lambda_{2s} - \frac{16}{\alpha_s^3\Lambda_{2s}} + \frac{4i\Lambda_{ds}}{\alpha_s^2 H\Lambda_{2s}}\Delta_s, \tag{79}$$

$$\tilde{\mathscr{D}}_{1v} = \Lambda_{2v} - \frac{16}{\alpha_v^3\Lambda_{2v}} + \frac{4i\Lambda_{dv}}{\alpha_v^2 H\Lambda_{2v}}\Delta_v. \tag{80}$$

From Eqs. (56) and (75), the upstream conditions for $\tilde{A}_s$ and $\tilde{A}_v$ are found as

$$\tilde{A}_s \to \hat{A}_s e^{i\frac{\Delta_s}{c_s}x_1}, \quad \tilde{A}_v \to \hat{A}_v e^{i\frac{\Delta_v}{c_v}x_1} \quad \text{as} \quad x_1 \to -\infty, \tag{81}$$

where $\hat{A}_s$ and $\hat{A}_v$ are constants representing the rescaled initial amplitudes. Inserting Eqs. (75) and (81) into Eqs. (53) and (54), we obtain the upstream conditions for $\tilde{Q}^{\pm}_{1,0}$, $\tilde{Q}^{\pm}_{0,1}$, $\tilde{Q}^{\pm}_{-1,0}$, and $\tilde{Q}^{\pm}_{0,-1}$,

Published under license by AIP Publishing

$$\tilde{Q}^{\pm}_{1,0} = \tilde{Q}^{\pm *}_{-1,0} \tag{82}$$

$$\sim \mp i\Delta_s\left(\frac{1}{c_s} - 1\right)\tilde{A}_s \int_0^\infty e^{-\frac{1}{3}\tilde{\lambda}\alpha_s^2\zeta^3 - i\alpha_s\zeta\tilde{\eta}_\pm - i\Delta_s\left(\frac{1}{c_s}-1\right)\zeta} \mathrm{d}\zeta, \tag{83}$$

$$\tilde{Q}^{\pm}_{0,1} = \tilde{Q}^{\pm *}_{0,-1} \tag{84}$$

$$\sim -i\Delta_v\left(\frac{1}{c_v} - 1\right)\tilde{A}_v \int_0^\infty e^{-\frac{1}{3}\tilde{\lambda}\alpha_v^2\zeta^3 - i\alpha_v\zeta\tilde{\eta}_\pm - i\Delta_v\left(\frac{1}{c_v}-1\right)\zeta} \mathrm{d}\zeta. \tag{85}$$

For all unseeded components, we take $\tilde{Q}^{\pm}_{m,n} = 0$ as $x_1 \to -\infty$.

Before turning to numerical solutions, we would like to make two observations. First, the nonlinear terms in the present problem are, due to their simple form, evaluated in the spectral space. In general, a pseudo-spectral evaluation would be more efficient in which case one calculates the flow field and the nonlinear term, $N(\theta_s, \theta_v)$ say, in the physical space, and then takes Fourier transform of N with respect to θ_s and θ_v to obtain[46]

$$\widehat{N}_{mn} = \frac{1}{(2\pi)^2}\int_{\mathrm{T}^2} N(\theta_s, \theta_v) e^{i(m\theta_s + n\theta_v)} \mathrm{d}\theta_s \mathrm{d}\theta_v, \tag{86}$$

which is needed in the downstream marching step. The conversions between physical and spectral spaces can be implemented using the FFT (Fast Fourier Transform) algorithm. Second, the representation of a quasi-periodic disturbance in terms of suitable phase variables on a torus, together with FFT, can be adapted in the NPSE approach[40] as well. This would enable that methodology, which has hitherto been restricted to modes with commensurate frequencies, to predict the nonlinear development of modes whose frequencies or wavenumbers are non-commensurate.

IV. NUMERICAL RESULTS

A popular choice for the base-flow profile is the "Bickley jet," $\bar{U} = 1 - u_0\,\mathrm{sech}^2 y$, for which it is known analytically that $\alpha_s = 2$ and $\alpha_v = 1$. This profile is perhaps too special to be representative because the ratio $\alpha_s/\alpha_v = 2$ is an integer. We are interested in the general case, where α_s/α_v is not a rational number. The profile is taken to be

$$\bar{U}(y) = 1 - u_0 e^{-a_m y^2 - b_m y^4}, \tag{87}$$

which describes a wake behind a flat plate for suitable values of a_m and b_m, as was found by Wygnanski *et al.*[14] and Marasli *et al.*[15] in their experiments. Two cases are considered for the values of a_m and b_m,

$$\text{Case 1} \quad (a_m, b_m) = (0.637, 0.056),$$
$$\text{Case 2} \quad (a_m, b_m) = (0.780, 0.120).$$

Case 1 corresponds to the experiments of Marasli *et al.*,[14,15] while case 2 leads to a different ratio of the wavenumbers of the sinuous and varicose modes. Three values of u_0, 0.5, 0.2, and 0.05, are considered for the first case, and 0.2 is used for the second case. In the experiment,[15] the maximum value of the root mean square of the perturbation velocity $\tilde{u}$ was found to be 11.7% of u_0, and so in our calculations, ε for both cases is $\varepsilon = 0.1u_0$, and $\varepsilon^{1/2}\Delta_s$ and $\varepsilon^{1/2}\Delta_v$ are taken to be 20% of $\alpha_s c$ and $\alpha_v c$, respectively.

A. Numerical solutions for ϕ_{1s} and ϕ_{1v}

The value of y_c for the chosen profile can be calculated analytically by solving for y_c from $\bar{U}''(y_c) = 0$. The values for y_c, c, $\bar{U}_c'$, $\bar{U}_c'''$, and $\bar{U}_c^{iv}$ are then evaluated analytically.

In order to obtain α_s, α_v, ϕ_{1s}, and ϕ_{1v}, Eqs. (12) and (13) are solved numerically by employing a shooting method, which involves solving the boundary-value problem as an initial-value problem plus an iterative procedure. We take the case of the sinuous mode ϕ_{1s} for illustration. Using the asymptotic behavior of ϕ_{1s}, the value of ϕ_{1s} and its derivative ϕ_{1s}' at a large distance, which is taken to be at $y = 8y_c$ to ensure that there is a grid point at y_c, are known up to the constants $r_{s\infty}$ and α_s. Since ϕ_{1s} is an even function, the lower boundary can be set at $y = 0$ with $\phi_{1s}'(0) = 0$.

Although the Rayleigh equation (12) is regular in the strict analytical sense because $\bar{U}''(y_c) = 0$, numerically the evaluation of $\bar{U}''/(\bar{U} - c)$ at $y = y_c$ must be treated with particular caution. We decide therefore to avoid a direct integration from the boundary to boundary and use instead a special version of a more general method that is applicable to non-inflectional neutral modes (which may exist on non-symmetric velocity profiles). With an initial guessed α_s and $r_{s\infty}$ being taken to be unity, the integration is carried out using a fourth-order Runge–Kutta scheme, up to the grid point above y_c, $y_c + h$ say. By equating $r_{s\infty}\phi_s(y_c + h)$ and $r_{s\infty}\phi_s'(y_c + h)$ with those obtained using the Frobenius solution (18), the values of a_s and $r_{s\infty}$ are determined. On the other hand, the Frobenius series (16) and (17) are used to set the initial conditions on the grid point below y_c for (ϕ_a, ϕ_a') and (ϕ_b, ϕ_b') separately, and the integration using RK4 to $y = 0$ is performed for each of them. The known boundary condition at $y = 0$ is then used to determine the value of a_s. The difference between the values of a_s obtained from the integrations above and below y_c needs to be made to vanish using the Newton–Raphson iteration on α_s. The iteration is repeated until the difference is less than 10^{-7}. The eigenfunction is finally calculated using the calculated α_s and is normalized by setting $\phi_{1s} = 1$ at $y = y_c$. The value of ϕ_{1s} for $y < 0$ follows from the symmetry condition. The varicose mode is found by the same procedure, except that $\phi_{1v}(0) = 0$.

In passing, it may be worth mentioning that if the critical level were not located at the inflection points, i.e., $U_c'' \neq 0$, one of the Frobenius solutions, ϕ_b, would contain a logarithmic term $\eta_\pm \ln|\eta_\pm|$, and a_s in Eq. (18) would take different values above and beneath y_c, with the difference (i.e., jump) being $\pi i U_c''/|U_c'|$. This is, of course, impossible since the values of a_s, as obtained by integrating the Rayleigh equation, are real valued. The above consideration offers an argument, alternative to that in Refs. 43 and 44 for the requirement that the critical levels be at the inflection points in a flow with a symmetric profile.

The code was validated by implementing it for the well-known "Bickley jet" profile for which there are exact solutions, $\alpha_s = 2$ and $\alpha_v = 1$, and the corresponding eigenfunctions are known analytically.

The calculated values of α_s and α_v for the base-flow two cases are given in Table I. The values of α_s, α_v, and their ratio α_s/α_v are most likely to be irrational (for the mathematical reason that rational numbers, though dense among real numbers, have measure zero). With α_s and α_v being approximated by decimal numbers of finite precision, the ratio $\alpha_v/\alpha_s = \omega_v/\omega_s$ is approximately 343/510 and 1213/1718 for cases 1 and 2, respectively, each of which is a fraction of a pair of two fairly large co-primes, and should be considered

Published under license by AIP Publishing

TABLE I. Calculated parameter values for the two base-flow profiles with $u_0 = 0.2$.

a_m	b_m	α_s	α_v	c	c_s	c_v	J_{2s}	J_{2v}
0.637	0.056	1.530	1.029	0.889	0.919 − 0.105i	1.021 − 0.060i	89.977	−40.086
0.780	0.120	1.718	1.213	0.892	0.927 − 0.117i	1.023 − 0.062i	82.577	−49.774

as an approximation of the irrational ratio. It follows that a disturbance consisting of the both modes would appear more aperiodic in the second case. The ratio of 343/510 ≈ 2/3 for the base-flow case is fairly close to the experimental value of 5/8.[14] The corresponding eigenfunctions ϕ_{1s} and ϕ_{1v} and their derivatives are shown in Fig. 1. Note that the shape of the eigenfunctions and their derivatives are independent of u_0. These are found to resemble those measured in experiments (see e.g., Fig. 17 in Ref. 14 and Figs. 4 and 10 in Ref. 15). The solutions for the second case look qualitatively similar and hence are not presented.

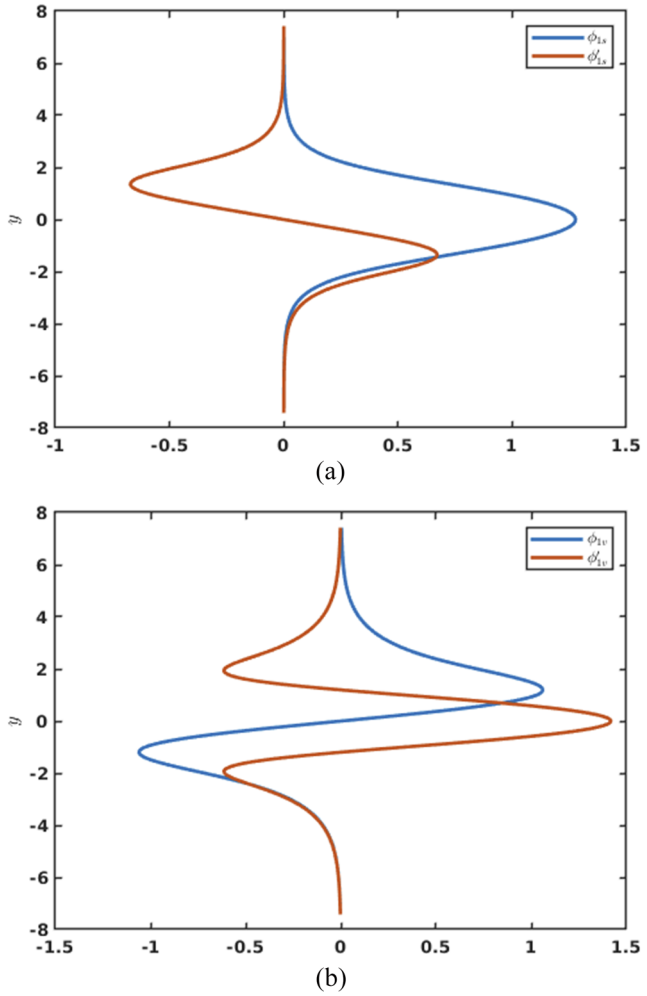


FIG. 1. Profiles of the eigenfunctions and their derivatives: (a) sinuous mode and (b) varicose mode.

B. Calculation of J_{1s}, J_{2s}, J_{1v}, and J_{2v}

The eigenfunctions, ϕ_{1s} and ϕ_{1v}, are now used to evaluate J_{1s}, J_{2s}, J_{1v}, and J_{2v}. Of these, J_{1s} and J_{1v} are calculated by a straightforward application of Simpson's rule. As ϕ_{1s} and ϕ_{1v} are independent of u_0 and so are J_{1s} and J_{1v}.

The calculation of J_{2s} and J_{2v} is slightly more involved due to the integrands being singular at $y = y_c$. In order to make the integrands suitable for numerical integration, the singularity has to be removed. This is done by identifying the $1/(y - y_c)$ term in the Laurent expansion of the integrands. This singular part is then subtracted from the numerically calculated integrand so that the integral can be evaluated using Simpson's rule. The contribution of the $1/(y - y_c)$ term to the integral is evaluated analytically as the Cauchy principal value and then added to the numerical evaluation of the integral to give the final result. J_{2s} and J_{2v} are dependent on (inversely proportional to) u_0, and their values, as well as the corresponding values for c_s and c_v, are displayed in Table II for profile 2.

C. Solving the evolution equations for $\tilde{A}_s$, $\tilde{A}_v$, and $\tilde{Q}^{\pm}_{m,n}$

With the coefficients in Eqs. (76)–(78) being evaluated using the base-flow parameters and eigenvalue modes found, the evolution equations for $\tilde{A}_s$, $\tilde{A}_v$, and $\tilde{Q}^{\pm}_{m,n}$ are solved using a predictor-corrector method adapted from Ref. 38. The functions $\tilde{A}_s$, $\tilde{A}_v$, and $\tilde{Q}^{\pm}_{m,n}$ are initialized using Eqs. (81)–(84). The integrals $\tilde{I}_{k,m,0}$ and $\tilde{I}_{k,0,n}$ in (77) and (78) are calculated using Simpson's rule. The derivatives of $\tilde{A}_s$ and $\tilde{A}_v$ in these equations are discretized using a fourth-order explicit Adams–Bashforth scheme for the predictor and a fourth-order implicit Adams–Moulton scheme for the corrector.[50] The vorticity equations (76) are discretized using the Crank–Nicolson scheme[50] on a grid consisting of 3600 points in the vertical direction with $\bar{\eta}_{\pm}$ between −60 and +60, and 54 000 points in the streamwise direction with x_1 between −10 and 30. The Fourier series (39) was truncated by retaining the terms with $|m| \le 15$ and $|n| \le 15$. The boundary conditions on $\tilde{Q}^{\pm}_{m,n}$ are set by Eqs. (B1)–(B7).

1. Evolution of A_s and A_v: Effects of initial amplitudes

Guided by the parameters in the experiment,[15] we choose $u_0 = 0.2$ for both cases, and the Reynolds number is taken to be 10 000 for the first case. This is greater than that in the experiment,[15] where $R \approx 4000$ and the focus was on linear instability. A higher R is found to lead to more significant nonlinear effects. For the second, the Reynolds number is set at an even higher value of 50 000 in order to increase nonlinearity.

Published under license by AIP Publishing

TABLE II. Calculated parameter values for $(a_m, b_m) = (0.637, 0.056)$.

u_0	c	$\bar{U}'_{c+}$	$\bar{U}'''_{c+}$	$\bar{U}^{iv}_{c+}$	c_s	c_v	J_{2s}	J_{2v}
0.5	0.722	0.377	−1.052	0.393	0.749 − 0.323i	1.064 − 0.186i	35.992	−16.042
0.2	0.889	0.151	−0.421	0.157	0.919 − 0.105i	1.021 − 0.060i	89.977	−40.086
0.05	0.972	0.038	−0.105	0.039	0.981 − 0.024i	1.005 − 0.014i	359.922	−160.417

Our primary interest is in the effect of the modal composition of the disturbance, which is controlled by the initial amplitudes A_s^0 and A_v^0; these are related to the rescaled initial amplitudes via

$$\hat{A}_s = \bar{U}'_{c_+} A_s^0, \quad \hat{A}_v = \bar{U}'_{c_+} A_v^0. \tag{88}$$

Four scenarios are considered. The first corresponds to a pure sinuous mode in which $A_v^0 = 0$ and A_s^0 is varied between 1 and 4. The second represents a pure varicose mode, where $A_s^0 = 0$ and A_v^0 is varied between values of 1 and 4. The third is for a fixed $A_v^0 = 1$ with A_s^0 varying between values of 1 and 4. Finally, the fourth is for a fixed $A_s^0 = 1$ with A_v^0 varying between 1 and 4.

The results for a pure sinuous mode are shown in Figs. 2(a) and 2(c) for the two chosen profiles. As expected, $|A_s|$ initially grows exponentially, but once $|A_s|$ has acquired a sufficiently large amplitude, nonlinearity comes into play, as a result of which $|A_s|$ undergoes oscillatory saturation. An increase in A_s^0 causes the saturation to take place earlier. Interestingly, the saturating amplitude in the nonlinear stage appears to differ much less relative to the change in the initial amplitude A_s^0. For instance, an increase in A_s^0 from 1 to 4 (or correspondingly $\ln|A_s|$ from −4.2 to −2.8) leads to a much smaller increase in the saturating amplitude from −2.2 to −2.0 only. Furthermore, the saturating amplitude starting with a higher A_s^0 does not always remain greater than that with a lower A_s^0 at all streamwise locations.

In the case of a pure varicose mode, shown in Figs. 2(b) and 2(d), $|A_v|$ initially grows exponentially followed by nonlinear oscillatory saturation. As with the case of a pure sinuous mode, the

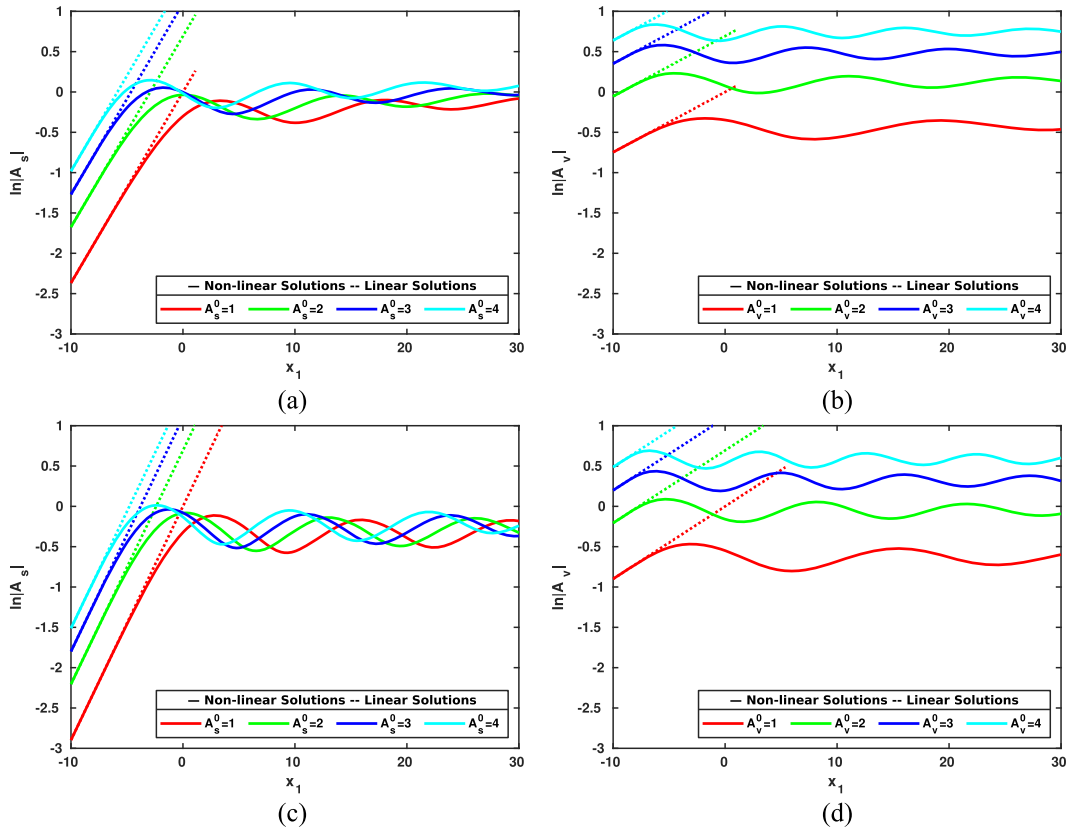


FIG. 2. Dependence of the amplitude evolution on the initial amplitudes for a pure sinuous mode [(a) and (c)] and a pure varicose mode [(b) and (d)]. First row: $(a_m, b_m) = (0.637, 0.056)$; second row: $(a_m, b_m) = (0.780, 0.120)$.

Published under license by AIP Publishing

saturation point moves upstream as A_v^0 is increased. In contrast to the pure sinuous case, however, a mode starting with higher A_v^0 maintains a larger amplitude at all streamwise locations. The difference in $|A_v|$ is broadly maintained as the mode evolves into the nonlinear stage.

The development of $\ln|A_s|$ and $\ln|A_v|$ for $A_v^0 = 1$ and different values of A_s^0 is shown in Figs. 3(a) and 3(b), respectively. The amplification of both $|A_s|$ and $|A_v|$ is initially exponential, as predicted by linear theory. However, the first deviation from the linear prediction occurs earlier than in the pure sinuous or varicose mode case. The final nonlinear saturation of $|A_s|$ and $|A_v|$ starts earlier for a larger A_s^0. In comparison with the purely sinuous case, the size of the oscillations in $|A_s|$ is significantly reduced. The sinuous mode broadly inhibits the varicose mode, as was found for the "Bickley jet" profile.[37] The degree of suppression increases monotonically with A_s^0 in the earlier nonlinear stage, but not in the later phase, where A_v may reach a higher level in the case of greater A_s^0, as shown in Figs. 3(b) and 3(d).

The ratio of $|A_v|$ to $|A_s|$ as a function of x_1 for $A_v^0 = 1$ and several values of A_s^0 is shown in Figs. 5(a) and 5(c) for the two base-flow profiles. $|A_s|$ and $|A_v|$ (upstream) differ considerably, e.g., $|A_v|$ may be larger than $|A_s|$. The ratio $|A_v|/|A_s|$ decreases with x_1 for all values of A_s^0 with the decrease being quicker for smaller A_s^0. At large x_1, $|A_v|/|A_s|$ tends to an almost constant value of about 0.4 for all A_s^0, suggesting that the starting amplitude has a limited effect on the ratio at a large x_1 and that the sinuous mode will always eventually dominate over the varicose mode.

The evolution of $\ln|A_s|$ and $\ln|A_v|$ for the final case of a fixed $A_s^0 = 1$ and different A_v^0 is shown in Figs. 4(a) and 4(b). The presence of the varicose mode leads to an earlier departure from the exponential growth compared to the purely sinuous case. For instance, the departure occurs at $x_1 \approx -3$ in the case of the pure sinuous mode for both base-flow profiles, but with $A_v^0 = 4$, the departure starts at $x_1 \approx -6$ and $x_1 \approx -7$ for the first and second profiles, respectively. The varicose mode initially inhibits the growth of the sinuous mode and causes the latter to saturate later. However, it leads to a significantly higher saturating amplitude of A_s in which sense the varicose mode enhances the sinuous mode eventually. The maximum of $\ln|A_s| \approx -2$ at $x_1 \approx 3$ for $A_v^0 = 0$ is compared to a maximum of $\ln|A_s| \approx -1.2$ at $x_1 \approx 20$ for $A_v^0 = 4$ for the first base-flow case. In the second base-flow case, the results are very similar with the maximum of $\ln|A_s| \approx -1.9$ at $x_1 \approx 2$ for $A_v^0 = 0$ compared to a maximum of $\ln|A_s| \approx -1.1$ at $x_1 \approx 20$ for $A_v^0 = 4$. Such a destabilizing effect of the varicose mode was not found in the previous study,[37] where A_v was held fixed. The

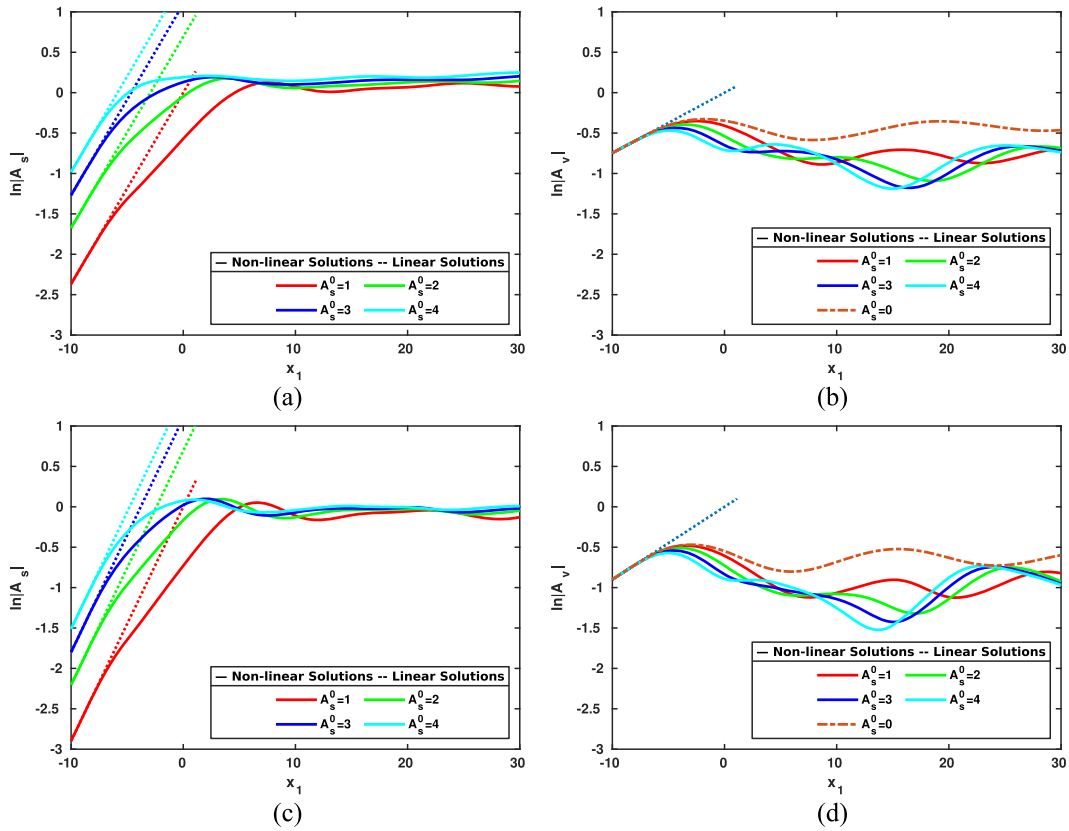


FIG. 3. Dependence of the amplitude evolution on A_s^0 with $A_v^0 = 1$. [(a) and (c)]: $\ln|A_s|$; [(b) and (d)]: $\ln|A_v|$. First row: $(a_m, b_m) = (0.637, 0.056)$; second row: $(a_m, b_m) = (0.780, 0.120)$.

Published under license by AIP Publishing

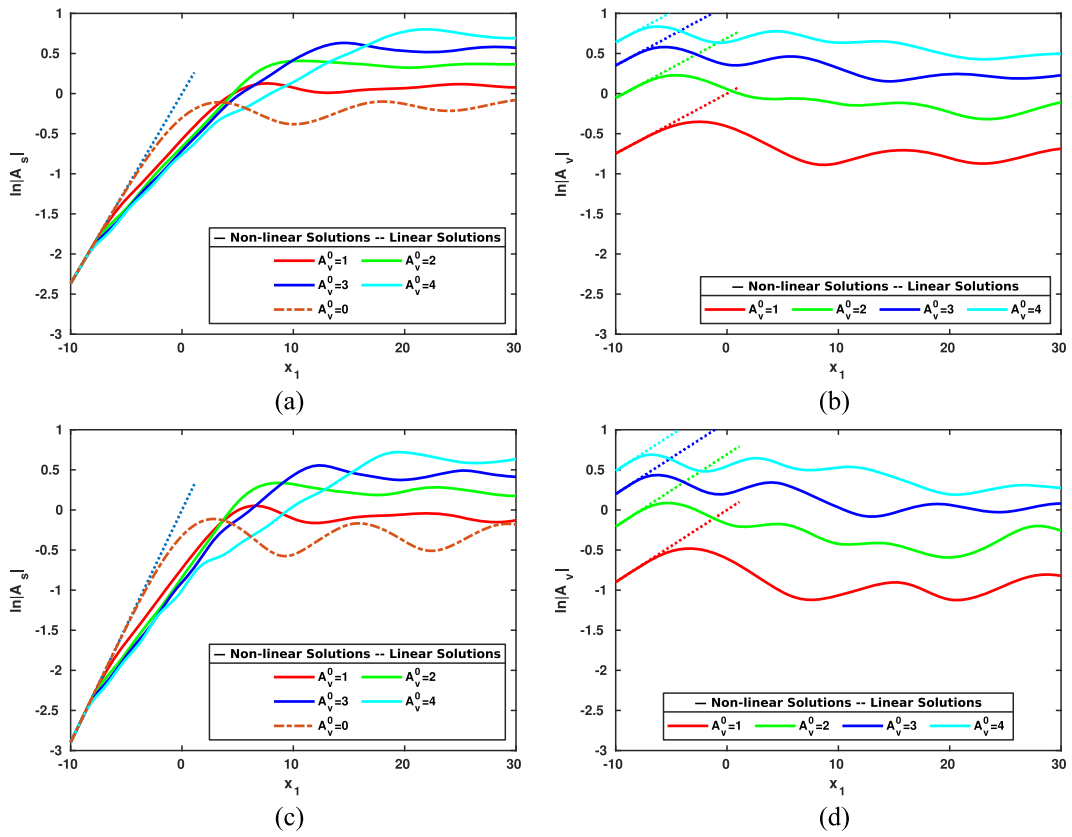


FIG. 4. Dependence of the amplitude evolution on A_v^0 with $A_s^0 = 1$. [(a) and (c)]: $\ln|A_s|$; [(b) and (d)]: $\ln|A_v|$. First row: (a_m, b_m) = (0.637, 0.056); second row: (a_m, b_m) = (0.780, 0.120).

oscillation in $|A_s|$ is reduced compared to the purely sinuous case. As in the purely varicose case, the value of $\ln|A_v|$ is mainly determined by A_v^0 with the difference in $\ln|A_v|$ between different values of A_v^0 being approximately the same for all x_1.

Finally, the ratio $|A_v|/|A_s|$ for a fixed $A_s^0 = 1$ and different A_v^0 is displayed in Figs. 5(b) and 5(d) for the two base-flow profiles. The overall dependence of $|A_v|/|A_s|$ on x_1 is the same as for the case of fixed $A_v^0 = 1$ and varying A_s^0. $|A_v|/|A_s|$ decreases at a decreasing rate with x_1 and oscillates about a constant value at large x_1. It shows again that even if $|A_v|$ is initially greater than $|A_s|$, the sinuous mode is dominant downstream.

The general trends predicted by our theory are in fair agreement with the experimental observations. The sinuous mode dominates over the varicose mode as has been observed, and specifically, the variation of $|A_v|/|A_s|$ with x_1 is qualitatively the same as that in the experiment.[15] The predicted ratio $|A_v|/|A_s|$ at large x_1 was found to be about 0.4–0.5; the measured value of 0.5 falls into this range of values. The result also helps explain the difficulty in obtaining a purely varicose disturbance[15] since even a varicose mode with an initial amplitude about four times that of the sinuous mode still leads to the eventual dominance of the sinuous mode. The final ratio of about 0.4–0.5 implies that a purely sinuous mode is also unlikely.

2. Dependence of A_s and A_v on the Reynolds number

The influence of the Reynolds number (i.e., viscosity) on the evolution of A_s and A_v is investigated for the first base-flow profile. We set $u_0 = 0.2$ and $A_s^0 = A_v^0 = 1$. The development of $\ln|A_s|$ and $\ln|A_v|$ for $R = 2500$, 5000, 10 000, and 20 000 and ∞ (the inviscid limit) is shown in Figs. 6(a) and 6(b). The viscous effects come into play only in the saturating stage. At lower Reynolds numbers, the amplitude $|A_s|$ is higher and appears to amplify algebraically as in the case of a pure sinuous mode.[33] The amplitude of the varicose mode, $|A_v|$, still exhibits appreciable oscillations about a mean value. When the Reynolds number is reduced, the oscillations in $|A_v|$ are reduced, while its mean value increases slightly. The amplitude ratio $|A_v|/|A_s|$ is shown in Fig. 6(c). The change in the Reynolds number has a slight effect on $|A_v|/|A_s|$, the final value of which is in the range of 0.4–0.5, in agreement with the measurement shown in Fig. 12 of Ref. 15, where the Reynolds number $R = 4000$.

D. Critical-layer vorticity

In addition to A_s and A_v, the critical-layer vorticity is another quantity of interest. The total vorticity in each critical layer is given by $U_c'^{\pm} + \varepsilon\Omega_c^{\pm}$, where $\Omega_c^{\pm}$ is defined as

Published under license by AIP Publishing

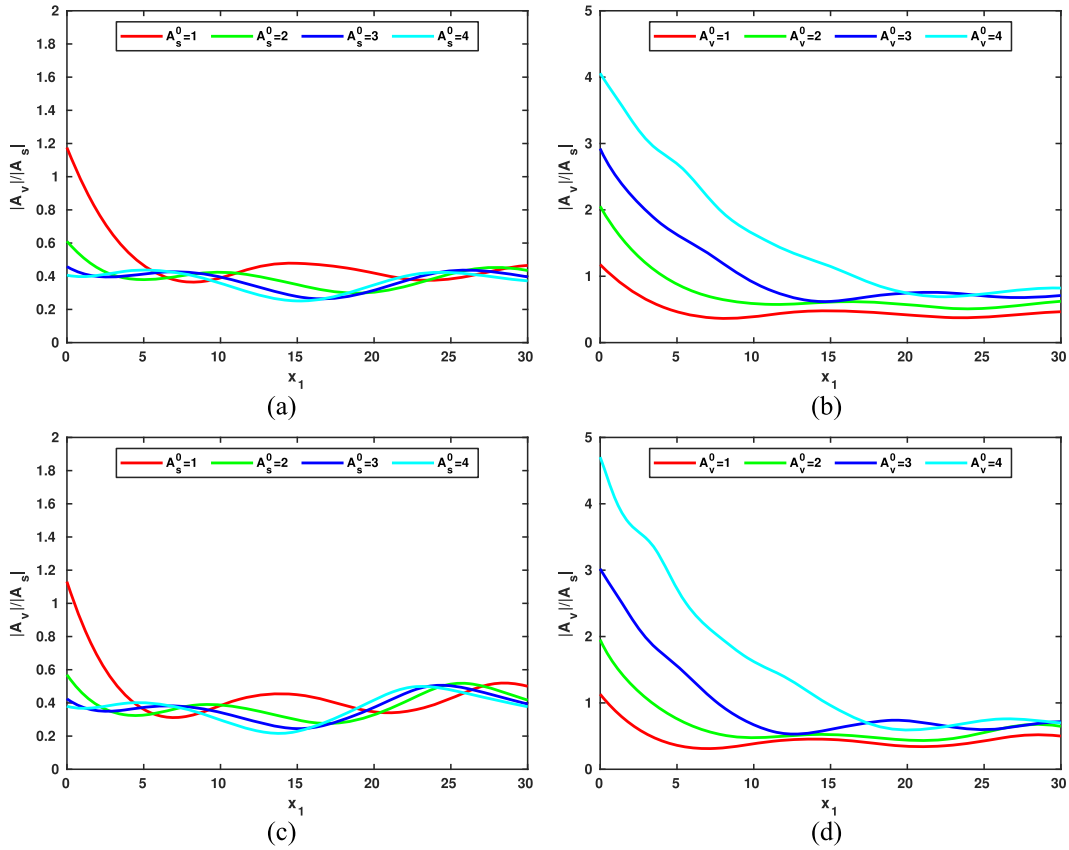


FIG. 5. Dependence of $|A_v|/|A_s|$ on the initial amplitudes for different A_s^0 with $A_v^0 = 1$ [(a) and (c)] and for different A_v^0 with $A_s^0 = 1$ [(b) and (d)]. First row: (a_m, b_m) = (0.637, 0.056); second row: (a_m, b_m) = (0.780, 0.120).

$$\Omega_c^{\pm} = \frac{1}{2} U_{c\pm}''' Y_{\pm}^2 + \left(\frac{\partial^2 \Psi_2^{\pm}}{\partial Y_{\pm}^2} + \frac{\partial^2 \Psi_1^{\pm}}{\partial \xi^2} \right)$$
$$= \frac{1}{2} U_{c\pm}''' Y_{\pm}^2 + \frac{U_{c\pm}'''}{U_{c\pm}'} \left(A_s e^{i\theta_s} \pm A_v e^{i\theta_v} + c.c. \right)$$
$$+ \sum_{m=-\infty}^{\infty} \sum_{n=-\infty}^{\infty} Q_{m,n}^{\pm} e^{i(m\theta_s + n\theta_v)}. \quad (89)$$

Here, use has been made of Eqs. (33), (36), and (39). The critical-layer vorticity is normalized in the same manner as $Q_{m,n}^{\pm}$, $\tilde{\Omega}_c^{\pm} = \tilde{U}_{c_\pm}'^2 / \tilde{U}_{c_\pm}''' \Omega_c^{\pm}$. In terms of the normalized variables, $\tilde{\Omega}_c^{\pm}$ is expressed as

$$\tilde{\Omega}_c^{\pm} = \frac{1}{2} \tilde{\eta}_{\pm}^2 \left(\pm \tilde{A}_s e^{i(\theta_s - \Delta_s t_1)} + \tilde{A}_v e^{i(\theta_v - \Delta_v t_1)} + c.c. \right)$$
$$+ \sum_{m=-\infty}^{\infty} \sum_{n=-\infty}^{\infty} \tilde{Q}_{m,n}^{\pm} e^{im(\theta_s - \Delta_s t_1) + in(\theta_v - \Delta_v t_1)}. \quad (90)$$

The unnormalized critical-layer vorticity is symmetric/antisymmetric in the purely sinuous/varicose case. This leads to the contour plots of the normalized vorticities in the upper and lower critical layer, $\tilde{\Omega}_c^{\pm}$, to be the same for the purely varicose case but offset by half a wavelength (i.e., 180° out of phase) in the purely sinuous case.

The critical-layer vorticity results for the base-flow case 1 are now discussed. The contours of $\tilde{\Omega}_c^{+}$ at $x_1 = -5$, 0, 5, 15, and 30 for the sinuous case mode $A_s^0 = 1$ are shown in the left column of Fig. 7. The contour pattern is repeated with a wavelength $2\pi/\alpha_s = 0.66 \times 2\pi$. The location $x_1 = -5$ is in the linear region, and the contours feature a fairly simple pattern without roll-up of the shear layer. At $x_1 = 0$, the evolution has entered the nonlinear regime, where $|A_s|$ is still growing with x_1 [see Fig. 2(a)]. The contours here show a considerable roll-up. The transverse size of the vortices has also increased from between $-4 \le \tilde{\eta} \le 4$ at $x_1 = -5$ to $-6 \le \tilde{\eta} \le 6$. At $x_1 = 5$, $|A_s|$ is close to its peak value and no longer exhibits a significant change. The vortices continue to roll up, and its transverse size remains approximately the same as that at $x_1 = 0$, but an appreciable difference is the appearance of a small-scale feature near the braid region of the vortices. At $x_1 = 15$ and 30, $|A_s|$ is changing less with x_1 than at upstream locations, and the contours of $\tilde{\Omega}_c^{+}$ relax to a simpler and more regular structure.

The right column of Fig. 7 shows the contours of $\tilde{\Omega}_c^{+}$ for the purely varicose case with $A_v^0 = 1$ at $x_1 = -5$, 0, 5, 15, and 30. As in the purely sinuous case, the spatial pattern in the contours respects

Published under license by AIP Publishing

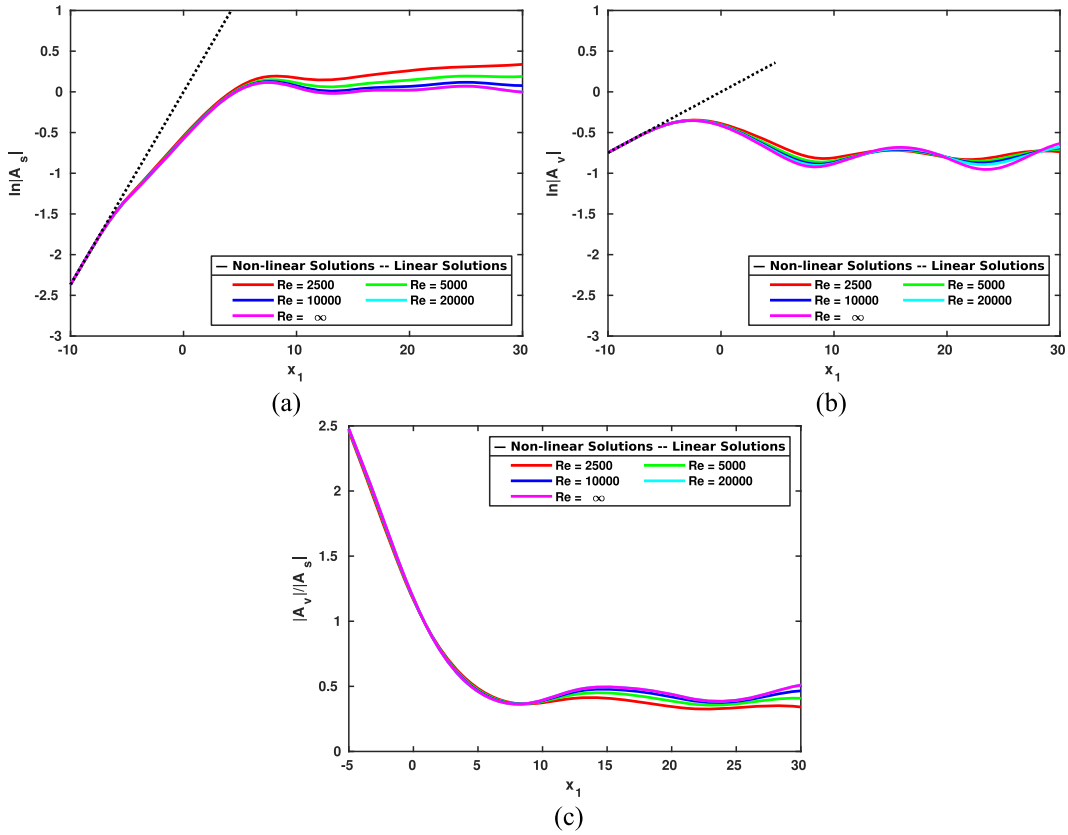


FIG. 6. Reynolds number effect on the amplitude evolution for $(a_m, b_m) = (0.637, 0.056)$: (a) $\ln|A_s|$, (b) $\ln|A_v|$, and (c) $|A_v|/|A_s|$.

periodicity now with the wavelength $2\pi/\alpha_v = 0.97 \times 2\pi$. At $x_1 = -5$, the varicose mode evolves nonlinearly, and thus, there is already a significant roll-up in the contours of $\bar{\Omega}_c^+$. The transverse vortex size in the varicose case is also greater than that in the pure sinuous case, occupying $-5 \le \bar{\eta} \le 5$, which is more-or-less maintained during the entire evolution. The contours of $\bar{\Omega}_c^+$ at $x_1 = 0$ show a broadly similar amount of roll-up to the situation at $x_1 = -5$. As in the purely sinuous case, the contours downstream, at $x_1 = 15$ and $x_1 = 30$, relax into a simpler pattern.

Next, we turn to the situation where both modes are present with $A_s^0 = A_v^0 = 1$. The symmetry/antisymmetry in the unnormalized critical-layer vorticity for the purely sinuous/varicose modes, respectively, is now broken due to the interaction between the two modes. As such, the contours of $\bar{\Omega}_c^+$ and $\bar{\Omega}_c^-$ are no longer identical or related simply by a phase shift. The contours of $\bar{\Omega}_c^+$ at $x_1 = -5$, 0, 5, 15, and 30 are shown in the central column of Fig. 7. The contours of $\bar{\Omega}_c^-$ (not shown) are broadly similar to those of $\bar{\Omega}_c^+$ for all x_1; however, appreciable differences exist.

At $x_1 = -5$, the vortices have already rolled up because of the presence of the varicose mode, which dominates over the sinuous mode and evolves nonlinearly. While the exact periodicity is lost, a quasi-periodic function is "almost periodic."[51] Presently, there is an almost repeating pattern of two vortices about every 4π in the contours of $\bar{\Omega}_c^+$. The two vortices have different sizes in ξ with one corresponding to the size of the vortices in the purely sinuous case and the other corresponding to their size in the purely varicose case. These two types of vortices will be referred to as "sinuous vortices" and "varicose vortices." There is more roll-up and complexity in the contours in this case compared to the purely sinuous and varicose cases.

At $x_1 = 0$, $|A_s|$ and $|A_v|$ are of comparable size with $|A_s|$ continuing to increase while $|A_v|$ having passed its peak value and is now decreasing [Figs. 4(a) and 4(b)]. The almost repeating patterns about every 4π in ξ are still present in the contours. However, the varicose vortex in the two-vortex structure at $x_1 = -5$ has been distorted, and there emerges a pattern alternating between an almost sinuous vortex and a stretched sinuous vortex within a varicose-vortex shaped envelope. This implies that as the sinuous mode starts to dominate over the varicose mode, it starts to define the pattern.

By $x_1 = 5$, the sinuous mode has almost reached its peak amplitude and become dominant over the varicose mode, which is still attenuating. The contours of $\bar{\Omega}_c^+$ almost repeat, approximately every 4π in ξ, now a pattern of three sinuous vortices. The middle vortex in the pattern is still wider in ξ and narrower in $\bar{\eta}_\pm$. With a non-zero amplitude, the varicose mode prevents the structure from reverting to that in the purely sinuous case. In addition, the transverse size

Published under license by AIP Publishing

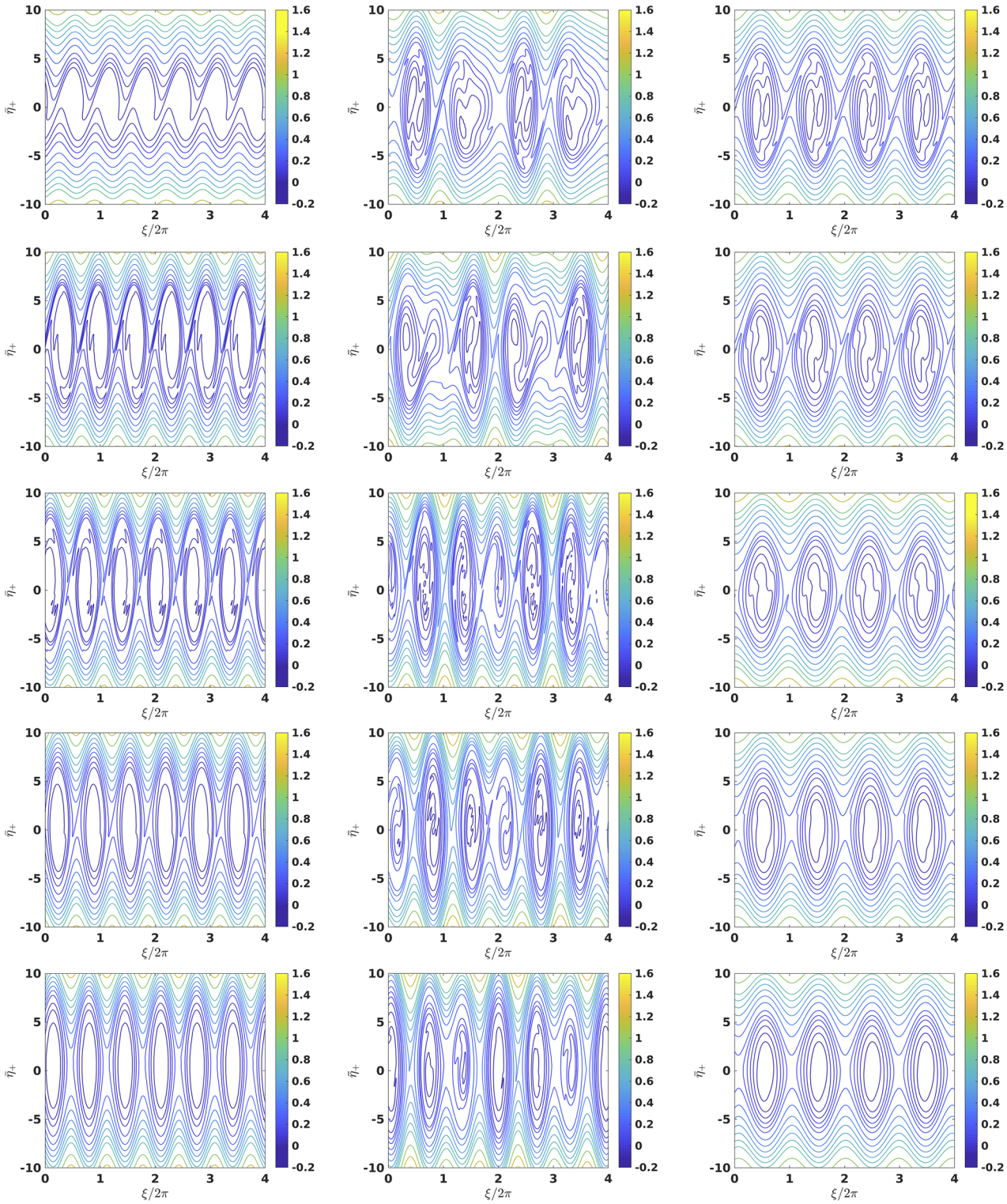


FIG. 7. Normalized upper critical-layer vorticity contours for (a_m, b_m) = (0.637, 0.056) at $x_1 = -5$ (first row), $x_1 = 0$ (second row), $x_1 = 5$ (third row), $x_1 = 15$ (fourth row), and $x_1 = 30$ (fifth row). The left/right column represents the pure sinuous/varicose mode case, whereas the middle column pertains to the case of mixed sinuous and varicose modes with $A_s^0 = A_v^0 = 1$.

Published under license by AIP Publishing

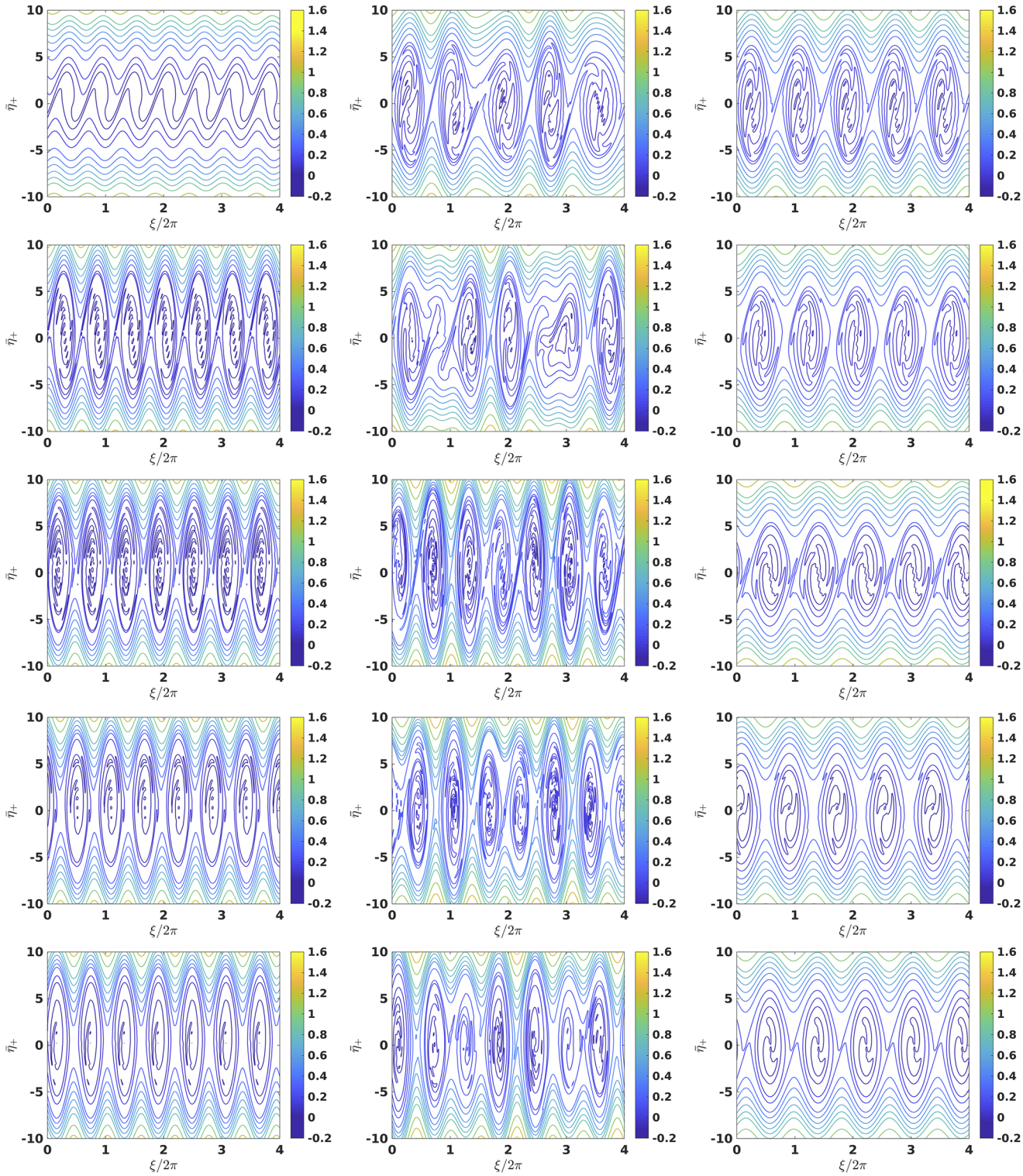


FIG. 8. Normalized upper critical-layer vorticity contours for (a_m, b_m) = (0.780, 0.120) at $x_1 = -5$ (first row), $x_1 = 0$ (second row), $x_1 = 5$ (third row), $x_1 = 15$ (fourth row), and $x_1 = 30$ (fifth row). The left/right column represents the pure sinuous/varicose mode case, whereas the middle column pertains to the case of mixed sinuous and varicose modes $A_s^0 = A_v^0 = 1$.

Published under license by AIP Publishing

of the vortices has increased compared to that at $x_1 = 0$, and an increased complexity of the contours can be observed despite the fact that the complexity would have been reduced if either of the two modes existed alone.

At $x_1 = 15$ and $x_1 = 30$, the contours are similar to those at $x_1 = 5$; however, the first two vortices in the three-vortex structure have become slightly wider in ξ and narrower in $\bar{\eta}_\pm$. This may be attributed to the fact that $|A_s|$ slightly decreases and $|A_v|$ slightly increases [see Figs. 4(a) and 4(b)]. The complexity of the contours is also slightly reduced compared to the situation at $x_1 = 5$ but is still much more remarkable than that in the case of a pure sinuous or varicose mode.

The critical-layer vorticity results for the second base-flow profile are presented in Fig. 8. The contours broadly resemble the first case. However, the quasi-periodicity, in the case of mixed sinuous and varicose modes, is more pronounced because the wavenumber (frequency) ratio is approximated by a fraction of a pair of larger coprimes. In addition, the effects of the relative strengths of the two modes at different x_1 on the critical-layer vorticities are reflected in the contours, as in the first case.

The contour patterns for the purely sinuous and varicose cases qualitatively resemble those in the "Bickley jet."[37] However, the case of combined sinuous and varicose modes is significantly different. The periodic structure due to the varicose mode being the subharmonic of the sinuous mode is now replaced by an almost repeating pattern consisting of two types of vortices, as discussed previously. This more complicated pattern bears a closer resemblance to the actual large coherent structures observed in the wake of a flat plate.[2,14] In particular, flow-visualization revealed vortices, which despite having a "prevailing wavelength," exhibit a "sufficient irregularity in their shape" while also lack any symmetry in the transverse direction (see Fig. 23 of Ref. 14). The irregularity and asymmetry were attributed to the co-existing varicose mode, the significant influence of which on the vortex pattern suggests that even when the sinuous mode is dominant in amplitude, the varicose mode should not be neglected.

E. Jumps of the harmonic components

The normalized streamwise velocity jumps across the upper and lower critical layers of the harmonic components are of interest because through them all harmonics, including those with the combinational frequencies ($m\omega_s + n\omega_v$), are generated simultaneously in the main shear layer. These jumps as functions of x_1 are calculated by applying Eqs. (41) and (42) with the normalized $\tilde{Q}^{\pm}_{m,n}$ and $\bar{\eta}_\pm$. The results for several values of m and n, as well as for the fundamental

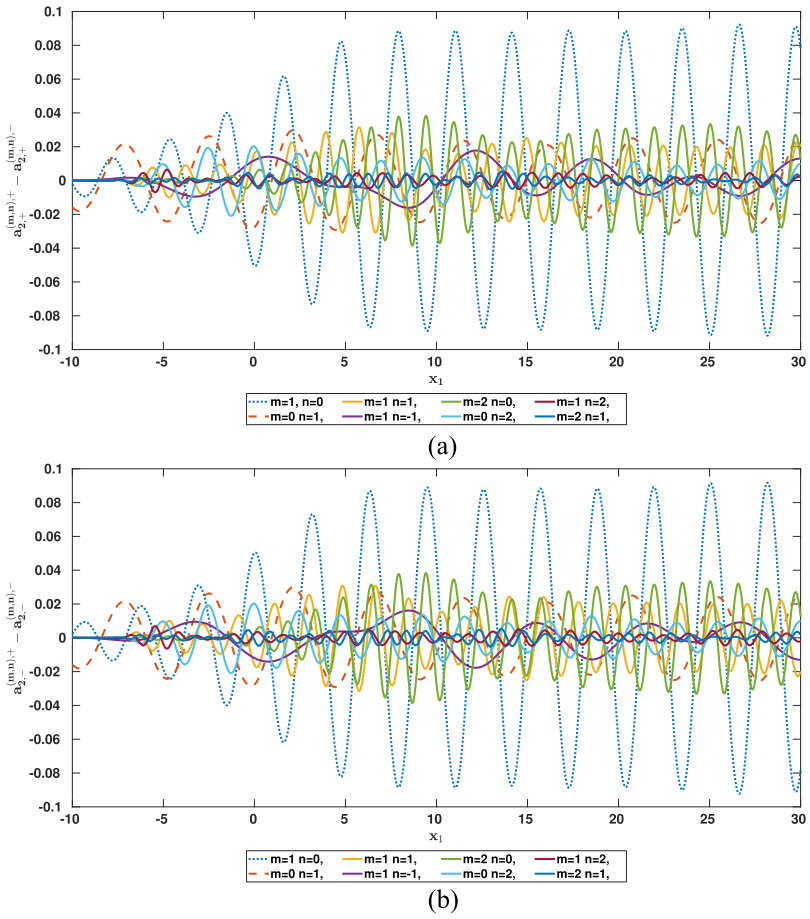


FIG. 9. Real part of the normalized jumps of the harmonics $(a_{2,\pm}^{(m,n),+} - a_{2,\pm}^{(m,n),-})$ across the upper critical layer (a) and the lower critical layer (b) for $(a_m, b_m) = (0.637, 0.056)$.

Published under license by AIP Publishing

components, are shown in Figs. 9(a) and 9(b); for brevity, only the real part of each jump is presented. The jumps for $(m, n) = (1, 0)$, $(1, 1)$, and $(1, -1)$ have opposite signs in the two critical layers, implying that the streamwise velocities of the corresponding harmonics are antisymmetric. The jumps for $(m, n) = (0, 1)$, $(1, 2)$, and $(2, 1)$ have the same sign in the two critical layers, implying that the streamwise velocities of these harmonics are symmetric. This agrees with the symmetry properties observed in the wake of a cylinder,[52] namely, if a harmonic is produced by the interaction of a symmetric and antisymmetric modes, then it will be antisymmetric. If instead a component is produced by two symmetric or two antisymmetric modes, then it will be symmetric.

The jumps in the non-fundamental components start to become appreciable from $x_1 \approx -7$, which coincides with the location at which $|A_s|$ and $|A_v|$ start to depart from the exponential growth. Initially, the jumps are largest for the $(0, 2)$, $(1, 1)$, and $(1, 2)$ components in that order, reflecting the initial dominance of the varicose mode. The $(1, 1)$ and $(1, 2)$ jumps do not grow significantly with x_1, however, and are suppressed back to low levels between $x_1 \approx -4$ and -2, and exhibit afterward relatively small-amplitude oscillations about zero. After the initial growth, the jump in the $(0, 2)$ component, which is the first harmonic of the varicose mode, retains roughly the same magnitude as x_1 increases until $x_1 \approx -3$. The jump in the $(2, 0)$ component, the first harmonic of the sinuous mode, is initially very small until $x_1 \approx 2$ at which point it starts to amplify until it becomes comparable in size with the jump in the fundamental varicose component $(0, 1)$ at $x_1 \approx 5$. The $(1, 1)$ component jump also grows with increasing x_1 but at a slower rate and stops growing at a slightly smaller value compared to the jump in the $(2, 0)$ component. The jump in the $(1, -1)$ component has the greatest variation in its size, ranging from being quite large and comparable with the $(1, 1)$ component to being small and of a magnitude closer to that of the $(1, 2)$ component. The disturbance in the main part of the shear layer consists of the fundamental and harmonic components. Since the two frequencies are incommensurable, the total time signal is quasi-periodic and may appear random-like.

The normalized streamwise velocity jumps for the second base-flow case are pretty similar to those for the first case and are not displayed here.

V. SUMMARY AND CONCLUSION

In this paper, a mathematical description was formulated to describe the nonlinear interaction and evolution of co-existing sinuous and varicose modes on a plane wake or jet. Previously, a strongly nonlinear non-equilibrium critical-layer theory has been developed for the specific flow profile of the "Bickley jet,"[37] where the ratio of the frequencies is an integer 2. That theory was too restrictive, and so we extended it to more general base-flow profiles for which the ratio of the sinuous and varicose mode frequencies is irrational. This allows for application to the profiles that fit better to the experimentally measured ones than the "Bickley jet" profile does. Due to the irrational ratio of the frequencies, the disturbances are quasi-periodic spatially and temporally, and the extension was achieved by expressing the solution as a function of two phase variables that is defined on a two-dimensional torus. The theory consists of the evolution equations governing the amplitudes of the sinuous and varicose modes coupled with the evolution equation governing disturbance vorticity in the critical layers.

Numerical calculations have been performed for two base-flow profiles. The first was chosen to represent the profile measured in the experiment.[14,15] The second one has the parameters chosen to show a more significant quasi-periodicity. The eigenvalues α_s and α_v, as well as their corresponding eigenfunctions ϕ_{1s} and ϕ_{1v}, were found to agree with the measurements.[14,15] The development of the amplitude of the sinuous and varicose modes depends on their initial amplitudes. In the purely sinuous case, an increase in the initial amplitude shifts the saturation location upstream, but the final saturating amplitude changes only moderately. In contrast, for the case of a pure varicose mode, an increase in its initial amplitude causes earlier saturation too, but the varicose mode amplitude is increased at all streamwise locations by almost the same amount. When the sinuous and varicose modes co-exist, the former broadly suppresses the latter but also renders the saturation of the latter highly oscillatory. As in the case of a pure sinuous mode, increasing the initial amplitude of the sinuous mode leads to earlier saturation, but only a slightly higher saturating amplitude. At the same time, the varicose mode is inhibited more severely in the earlier stage and exhibits stronger oscillations in the later stage. In contrast, increasing the initial amplitude of the varicose mode leads to a uniform increase in its intensity at all subsequent streamwise locations, including an appreciably greater saturating amplitude. These results showed agreement with the trends observed in the previous experimental and theoretical studies.[14,15,37] The presence of the varicose mode initially inhibits the sinuous mode, but surprisingly and significantly, it lends the latter a greater saturating amplitude in the late stage in which sense the varicose mode enhances the sinuous mode and plays a somewhat destabilizing or catalyzing role.

For a wide range of initial amplitudes of the sinuous mode, the amplitude ratio of the varicose and sinuous modes tends to an almost constant value, indicating a persistent coexistence of the two. This ratio was found to be dependent on the initial amplitude of the varicose mode, but the dependence is rather weak. The sinuous mode becomes dominant eventually. The Reynolds number affects the sinuous and varicose modes only in the nonlinear saturating stage. Decreasing the Reynolds number leads to larger amplitudes of both modes and inhibits the oscillations in their amplitudes. The relative size of the two modes showed a very little dependence on the Reynolds number.

The critical-layer vorticities were calculated and their development was monitored. In either the purely sinuous or varicose case, the vorticities exhibit a well-defined streamwise wavelength. The contours of the vorticity roll up to form a spanwise roller structure characteristic of transitional free shear layers, with the complexity of the contours increasing with x_1 until the amplitude of the mode has reached its peak value, after which they relax to somewhat simpler patterns. The size of the vortices increases up to the location where the amplitude peaks.

The critical-layer vorticity in the case with both modes present showed considerably more complexity than that in either of the single-mode cases. The structures were no longer periodic, nevertheless, exhibiting almost repeating features. In the fully rolled-up stage, the vortices appear to be rather different from those in either case of a pure sinuous or varicose mode, with the rollers featuring a more small-scale complexity and persisting for much

Published under license by AIP Publishing

longer distances. This is even true at downstream locations where the sinuous mode dominates over the varicose counterpart. With an increased complexity, the vortices resembled closely those observed in experiment.[14]

Finally, the harmonic components in the streamwise velocity jumps across the upper and lower critical layers were calculated. Significant jumps were found to occur when the amplitudes of the sinuous and varicose modes depart from the linear behavior. The lack of a general time and streamwise periodicity in all of the components implies the quasi-periodic nature of the total velocity perturbation.

Several avenues for future work emerge from this study. The first would be to solve the evolution system numerically for spatial-temporally modulated wavetrains consisting of a discrete set or a continuum of side-band components of the sinuous and varicose modes. The interactions of such a more general form of disturbances are an important process in the transition, as was shown by experiments.[8–11,53] Furthermore, it is of interest to have more precise values for the parameters characterizing the base flow and disturbances in experiments so that quantitative comparisons can be made. The numerical computations in this study have focused on plane wakes, but it would be possible to perform calculations and make comparisons with experimental results for a plane jet.

The present formulation was directed at laminar wakes and jets, but it is well known that coherent structures exist in the turbulent counterpart of these flows, and moreover, these structures are akin to the instability modes supported by the time-averaged mean velocity profile. It would be interesting to adapt the present formulation to model the nonlinear dynamics of these structures, as was done for a mixing layer.[47] This would require the triple decomposition,[54] which splits the instantaneous flow field into a sum of the time-averaged mean flow, the coherent structures, and the small-scale turbulence. It is then important to account for the strong non-parallelism due to the fast spreading of the turbulent mean flow.[47] Furthermore, the introduction of an eddy viscosity type of closure model would lead to the appearance of additional terms.

Finally, nonlinear interactions of instability waves in broad spectral bands consisting of non-commensurable frequencies or wavenumbers are characteristic of natural transition,[55] but appropriate mathematical tools to study them are not yet available. The idea of representing quasi-periodic disturbances in terms of phase variables on a torus of high dimension could be applied in either a nonlinear critical-layer framework[34,49] or a NPSE approach[40] to develop extended methodologies capable of handling such general forms of disturbances.

ACKNOWLEDGMENTS

The authors would like to thank the reviewers for their comments and suggestions, which helped improve this paper. K.M. would like to acknowledge funding for this work from the EPSRC CDT for fluid dynamics across scales (Grant No. EP/L016230/1).

APPENDIX A: DERIVATION OF EQ. (68)

First, applying $\mathscr{D}_0$ to both sides of Eq. (66) while omitting the $O(1/H)$ term and making use of Eqs. (48) and (59), we obtain

$$\left[\Lambda_{1s}\frac{\partial}{\partial t_1}+\Lambda_{2s}\frac{\partial}{\partial x_1}\right]\mathscr{D}_0\tilde{A}_s=\int_{-H}^{H}\mathscr{D}_0\tilde{Q}^{+}_{1,0}\mathrm{d}\bar{\eta}_+-\int_{-H}^{H}\mathscr{D}_0\tilde{Q}^{-}_{1,0}\mathrm{d}\bar{\eta}_-$$
$$=-4H\mathscr{D}_0\tilde{A}_s-i\alpha_s I_{1,1,0}+O(H^{-1}), \quad \text{(A1)}$$

where $I_{1,1,0}$ and subsequently terms of the form $I_{k,m,0}$ are defined as

$$I_{k,m,0}=\int_{-H}^{H}\bar{\eta}_+^k\tilde{Q}^{+}_{m,0}\mathrm{d}\bar{\eta}_+-\int_{-H}^{H}\bar{\eta}_-^k\tilde{Q}^{-}_{m,0}\mathrm{d}\bar{\eta}_-. \quad \text{(A2)}$$

Then, Eq. (A1) is re-arranged to

$$\Lambda_{2s}\mathscr{D}_0^2\tilde{A}_s=-\Lambda_{ds}\frac{\partial}{\partial t_1}\mathscr{D}_0\tilde{A}_s-4H\mathscr{D}_0\tilde{A}_s-i\alpha_s I_{1,1,0}+O(H^{-1}), \quad \text{(A3)}$$

where $\Lambda_{ds}=\Lambda_{1s}-\Lambda_{2s}$. This is substituted back into Eq. (66) to eliminate the $\mathscr{D}_0^2\tilde{A}_s$ term, leading to

$$\mathscr{D}_{1s}\mathscr{D}_0\tilde{A}_s=I_{0,1,0}-\Lambda_{ds}\frac{\partial\tilde{A}_s}{\partial t_1}+\frac{4iI_{1,1,0}}{\alpha_s H\Lambda_{2s}}+O(H^{-2}), \quad \text{(A4)}$$

where

$$\mathscr{D}_{1s}=\Lambda_{2s}-\frac{16}{\alpha_s^2\Lambda_{2s}}-\frac{4\Lambda_{ds}}{\alpha_s^2H\Lambda_{2s}}\frac{\partial}{\partial t_1}. \quad \text{(A5)}$$

Equation (A4) is now of first order with respect to x_1, but the domain truncation error is $O(H^{-2})$. Applying $\mathscr{D}_0$ to Eq. (A4) then gives

$$\mathscr{D}_{1s}\mathscr{D}_0^2\tilde{A}_s=-4H\mathscr{D}_0\tilde{A}_s-iI_{1,1,0}-\Lambda_{ds}\frac{\partial\mathscr{D}_0\tilde{A}_s}{\partial t_1}$$
$$+\frac{4}{\alpha_s H\Lambda_{2s}}\left(I_{2,1,0}-\tilde{A}_s^*I_{0,2,0}\right)+O(H^{-2}). \quad \text{(A6)}$$

Finally, acting $\mathscr{D}_{1s}$ on Eq. (66) and substituting Eq. (A6) into the resultant equation, we obtain the truncated equation [Eq. (68)].

APPENDIX B: BOUNDARY CONDITIONS FOR $\tilde{Q}^{\pm}_{m,n}$ (m = 0, ±1, ±2 AND n = 0, ±1, ±2)

$$\tilde{Q}^{\pm}_{1,0}=\tilde{Q}^{\pm *}_{-1,0}\to\pm\left(\frac{i}{\bar{\eta}_\pm\alpha_s}-\frac{\mathscr{D}_s}{\bar{\eta}_\pm^2\alpha_s^2}-\frac{i\mathscr{D}_s^2}{\bar{\eta}_\pm^3\alpha_s^3}\right)\mathscr{D}_s\tilde{A}_s+O(\bar{\eta}_\pm^{-4}), \quad \text{(B1)}$$

$$\tilde{Q}^{\pm}_{0,1}=\tilde{Q}^{\pm *}_{0,-1}\to\left(\frac{i}{\bar{\eta}_\pm\alpha_v}-\frac{\mathscr{D}_v}{\bar{\eta}_\pm^2\alpha_v^2}-\frac{i\mathscr{D}_v^2}{\bar{\eta}_\pm^3\alpha_v^3}\right)\mathscr{D}_v\tilde{A}_v+O(\bar{\eta}_\pm^{-4}), \quad \text{(B2)}$$

$$\tilde{Q}^{\pm}_{0,0}\to-\frac{1}{\bar{\eta}_\pm^2}\left(|\tilde{A}_s|^2+|\tilde{A}_v|^2\right)$$
$$+\frac{2i}{\bar{\eta}_\pm^3}\left(\frac{\tilde{A}_s\mathscr{D}_s{}^*\tilde{A}_s^*-c.c.}{\alpha_s}+\frac{\tilde{A}_v\mathscr{D}_v{}^*\tilde{A}_v^*-c.c.}{\alpha_v}\right)+O(\bar{\eta}_\pm^{-4}), \quad \text{(B3)}$$

$$\tilde{Q}^{\pm}_{1,1}=\tilde{Q}^{\pm *}_{-1,-1}\to\mp\frac{i}{(\alpha_s+\alpha_v)\bar{\eta}_\pm^3}\left(\frac{\alpha_s}{\alpha_v}\tilde{A}_s\mathscr{D}_v\tilde{A}_v+\frac{\alpha_v}{\alpha_s}\tilde{A}_v\mathscr{D}_s\tilde{A}_s\right)$$
$$+O(\bar{\eta}_\pm^{-4}), \quad \text{(B4)}$$

$$\tilde{Q}^{\pm}_{2,0}=\tilde{Q}^{\pm *}_{-2,0}\to-\frac{i}{2\alpha_s\bar{\eta}_\pm^3}\left(\tilde{A}_s\mathscr{D}_s\tilde{A}_s\right)+O(\bar{\eta}_\pm^{-4}), \quad \text{(B5)}$$

$$\tilde{Q}^{\pm}_{0,2}=\tilde{Q}^{\pm *}_{0,-2}\to-\frac{i}{2\alpha_v\bar{\eta}_\pm^3}\left(\tilde{A}_v\mathscr{D}_v\tilde{A}_v\right)+O(\bar{\eta}_\pm^{-4}), \quad \text{(B6)}$$

Published under license by AIP Publishing

$$\tilde{Q}^{\pm}_{1,-1} = \tilde{Q}^{\pm *}_{-1,1} \to \pm \frac{i}{(\alpha_s - \alpha_v)\tilde{\eta}^3_{\pm}} \left(\frac{\alpha_s}{\alpha_v} \tilde{A}_s \mathscr{D}_v{}^* \tilde{A}^*_v + \frac{\alpha_v}{\alpha_s} \tilde{A}^*_v \mathscr{D}_s \tilde{A}_s \right) + O(\tilde{\eta}^{-4}_{\pm}). \quad \text{(B7)}$$

DATA AVAILABILITY

The data that support the findings of this study are available within the article.

REFERENCES

[1] D. D. Papailiou and P. S. Lykoudis, "Turbulent vortex streets and the entrainment mechanism of the turbulent wake," J. Fluid Mech. **62**, 11–31 (1974).
[2] F. A. Roberts and A. Roshko, "Effects of periodic forcing on mixing in turbulent shear layers and wakes," AIAA Paper No. 1985-0570, 1985.
[3] P. Jordan and T. Colonius, "Wave packets and turbulent jet noise," Annu. Rev. Fluid Mech. **45**, 173–195 (2013).
[4] H. Sato and K. Kuriki, "The mechanism of transition in the wake of a thin flat plate placed parallel to a uniform flow," J. Fluid Mech. **11**, 321–352 (1961).
[5] D. T. Papageorgiou and F. T. Smith, "Linear instability of the wake behind a flat plate placed parallel to a uniform stream," J. Fluid Mech. **208**, 67–89 (1989).
[6] H. Sato, "The stability and transition of a two-dimensional jet," J. Fluid Mech. **7**, 53–80 (1960).
[7] G. E. Mattingly and W. O. Criminale, "The stability of an incompressible two-dimensional wake," J. Fluid Mech. **51**, 233–272 (1972).
[8] H. Sato and H. Saito, "Fine-structure of energy spectra of velocity fluctuations in the transition region of a two-dimensional wake," J. Fluid Mech. **67**, 539–559 (1975).
[9] R. W. Miksad, F. L. Jones, and E. J. Powers, "Measurements of nonlinear interactions during natural transition of a symmetric wake," Phys. Fluids **26**, 1402–1409 (1983).
[10] H. Sato, "An experimental study of non-linear interaction of velocity fluctuations in the transition region of a two-dimensional wake," J. Fluid Mech. **44**, 741–765 (1970).
[11] Ch. P. Ritz, E. J. Powers, R. W. Miksad, and R. S. Solis, "Nonlinear spectral dynamics of a transitioning flow," Phys. Fluids **31**, 3577–3588 (1988).
[12] C. M. Ho and P. Huerre, "Perturbed free shear layers," Annu. Rev. Fluid Mech. **16**, 365–422 (1984).
[13] H. Maekawa, N. N. Mansour, and J. C. Buell, "Instability mode interactions in a spatially developing plane wake," J. Fluid Mech. **235**, 223–254 (1992).
[14] I. Wygnanski, F. Champagne, and B. Marasli, "On the large-scale structures in two-dimensional, small-deficit, turbulent wakes," J. Fluid Mech. **168**, 31–71 (1986).
[15] B. Marasli, F. H. Champagne, and I. J. Wygnanski, "Modal decomposition of velocity signals in a plane, turbulent wake," J. Fluid Mech. **198**, 255–273 (1989).
[16] A. K. M. F. Hussain and C. A. Thompson, "Controlled symmetric perturbation of the plane jet: An experimental study in the initial region," J. Fluid Mech. **100**, 397–431 (1980).
[17] M. Matsubara, P. H. Alfredsson, and A. Segalini, "Linear modes in a planar turbulent jet," J. Fluid Mech. **888**, A26 (2020).
[18] G. L. Brown and A. Roshko, "On density effects and large structure in turbulent mixing layers," J. Fluid Mech. **64**, 775–816 (1974).
[19] D. G. Crighton and M. Gaster, "Stability of slowly diverging jet flow," J. Fluid Mech. **77**, 397–413 (1976).
[20] B. Marasli, F. H. Champagne, and I. J. Wygnanski, "On linear evolution of unstable disturbances in a plane turbulent wake," Phys. Fluids A **3**, 665–674 (1991).
[21] J. T. C. Liu, "Finite-amplitude instability of the compressible laminar wake. Weakly nonlinear theory," Phys. Fluids **12**, 1763–1774 (1969).
[22] S. A. Maslowe, "Weakly nonlinear stability of a viscous free shear layer," J. Fluid Mech. **79**, 689–702 (1977).
[23] J. T. Stuart, "On the non-linear mechanics of wave disturbances in stable and unstable parallel flows Part 1. The basic behaviour in plane Poiseuille flow," J. Fluid Mech. **9**, 353–370 (1960).
[24] J. Watson, "On the non-linear mechanics of wave disturbances in stable and unstable parallel flows Part 2. The development of a solution for plane Poiseuille flow and for plane Couette flow," J. Fluid Mech. **9**, 371–389 (1960).
[25] J. T. C. Liu and L. Lees, "Finite-amplitude instability of the compressible laminar wake. Strongly amplified disturbances," Phys. Fluids **13**, 2932–2938 (1970).
[26] D. R.-S. Ko, T. Kubota, and L. Lees, "Finite disturbance effect on the stability of a laminar incompressible wake behind a flat plate," J. Fluid Mech. **40**, 315–341 (1970).
[27] J. T. C. Liu and P. M. Gururaj, "Finite-amplitude instability of the compressible laminar wake: Comparison with experiments," Phys. Fluids **17**, 532–543 (1974).
[28] D. T. Papageorgiou and F. T. Smith, "Nonlinear instability of the wake behind a flat plate placed parallel to a uniform stream," Proc. R. Soc. London, Ser. A **419**, 1–28 (1988).
[29] S. M. Churilov and I. G. Shukhman, "Note on weakly nonlinear stability theory of a free mixing layer," Proc. R. Soc. London, Ser. A **409**, 351–367 (1987).
[30] P. Huerre, "On the Landau constant in mixing layers," Proc. R. Soc. London, Ser. A **409**, 369–381 (1987).
[31] P. Huerre and J. F. Scott, "Effects of critical layer structure on the nonlinear evolution of waves in free shear layers," Proc. R. Soc. London, Ser. A **371**, 509–524 (1980).
[32] M. E. Goldstein and S. J. Leib, "Nonlinear roll-up of externally excited free shear layers," J. Fluid Mech. **191**, 481–515 (1988).
[33] M. E. Goldstein and L. S. Hultgren, "Nonlinear spatial evolution of an externally excited instability wave in a free shear layer," J. Fluid Mech. **197**, 295–330 (1988).
[34] X. Wu, "Nonlinear theories for shear flow instabilities: Physical insights and practical implications," Annu. Rev. Fluid Mech. **51**, 451–485 (2019).
[35] D. Rockwell, A. Ongoren, and M. Unal, "Trailing-edge/end interactions and instabilities-some recent progress," in *Shear Flow-Structure Interaction Phenomena: Proceedings of the Winter Annual Meeting, Miami Beach, FL, November 17–22, 1985 (A86-28630 12-34)* (American Society of Mechanical Engineers, New York, 1985), pp. 27–36.
[36] H. Sato and H. Saito, "Artificial control of the laminar-turbulent transition of a two-dimensional wake by external sound," J. Fluid Mech. **84**, 657–672 (1978).
[37] S. J. Leib and M. E. Goldstein, "Nonlinear interaction between the sinuous and varicose instability modes in a plane wake," Phys. Fluids A **1**, 513–521 (1989).
[38] X. Wu and F. Tian, "Spectral broadening and flow randomization in free shear layers," J. Fluid Mech. **706**, 431–469 (2012).
[39] X. Wu, "On an active resonant triad of mixed modes in symmetric shear flows: A plane wake as a paradigm," J. Fluid Mech. **317**, 337–368 (1996).
[40] T. Herbert, "Parabolized stability equations," Annu. Rev. Fluid Mech. **29**, 245–283 (1997).
[41] P. Huerre and P. A. Monkewitz, "Local and global instabilities in spatially developing flows," Annu. Rev. Fluid Mech. **22**, 473–537 (1990).
[42] J.-M. Chomaz, "Global instabilities in spatially developing flows: Non-normality and nonlinearity," Annu. Rev. Fluid Mech. **37**, 357–392 (2005).
[43] C. C. Lin, "Some physical aspects of the stability of parallel flows," Proc. Natl. Acad. Sci. U. S. A. **40**, 741 (1954).
[44] J. R. Foote and C. C. Lin, "Some recent investigations in the theory of hydrodynamic stability," Quart. Appl. Math. **8**, 265–280 (1950).
[45] R. Haberman, "Critical layers in parallel flows," Stud. Appl. Math. **51**, 139–161 (1972).
[46] F. Schilder, W. Vogt, S. Schreiber, and H. M. Osinga, "Fourier methods for quasi-periodic oscillations," Int. J. Numer. Methods Eng. **67**, 629–671 (2006).
[47] X. Wu and X. Zhuang, "Nonlinear dynamics of large-scale coherent structures in turbulent free shear layers," J. Fluid Mech. **787**, 396–439 (2016).
[48] D. J. Benney and R. F. Bergeron, Jr., "A new class of nonlinear waves in parallel flows," Studies Appl. Math. **48**, 181–204 (1969).

Published under license by AIP Publishing

[49]I. G. Shukhman, "Quasi-linear instability theory for a weakly supercritical zonal shear flow on the β-plane," Geophys. Astrophys. Fluid Dyn. **39**, 105–118 (1987).
[50]E. Hairer, S. P. Nørsett, and G. Wanner, *Solving Ordinary Differential Equations I* (Springer, 1993).
[51]A. S. Besicovitch, *Almost Periodic Functions* (Dover Publications, Inc., New York, 1955), p. XIII.
[52]H. Mansy and D. R. Williams, "Symmetry of interacting modes in a cylinder wake," Phys. Fluids A **3**, 2047–2049 (1991).
[53]R. W. Miksad, F. L. Jones, E. J. Powers, Y. C. Kim, and L. Khadra, "Experiments on the role of amplitude and phase modulations during transition to turbulence," J. Fluid Mech. **123**, 1–29 (1982).
[54]W. C. Reynolds and A. K. M. F. Hussain, "The mechanics of an organized wave in turbulent shear flow. Part 3. Theoretical models and comparisons with experiments," J. Fluid Mech. **54**, 263–288 (1972).
[55]W. Würz, D. Sartorius, V. I. Borodulin, and Y. S. Kachanov, "Weakly-nonlinear interactions of broadband Tollmien–Schlichting waves in a non-self-similar boundary layer on an airfoil," Eur. J. Mech. B Fluids **77**, 48–70 (2019).

Published under license by AIP Publishing